ICARUS 117, 173–196 (1995)

A Global Survey of Possible Subduction Sites on Venus

G. SCHUBERT

Department of Earth and Space Sciences, Institute of Geophysics and Planetary Physics, University of California, Los Angeles, California 90095-1567
E-mail: gschubert@mgnvax.ess.ucla.edu

AND

D. T. SANDWELL

Institute of Geophysics and Planetary Physics, Scripps Institute of Oceanography, La Jolla, California 92093-0225

Received November 21, 1994; revised May 5, 1995

About 10,000 km of trenches in chasmata and coronae have been identified as possible sites of retrograde subduction on Venus. All the sites have narrow deep trenches elongate along strike with arcuate planforms, ridge–trench–outer rise topographic profiles typical of terrestrial subduction zones, large outer rise curvatures $>10^{-7}$ m^{-1}, fractures parallel to the strike of the trench on the outer trench wall and outer rise, and no cross-strike fractures across the trench. Both the northern and southern margins of Latona Corona are possible subduction sites. Identification of a major graben between the two principal outer ridges in southern Latona Corona is evidence of back-arc extension in the corona; the amount of extension is estimated to be more than 2–11 km. The moment exerted by the ridges of southern Latona Corona is insufficient to bend the lithosphere into the observed outer rise shape; a negatively buoyant subducted or underthrust slab is needed. Depending on the unknown trench migration rate, lithospheric subduction can make a significant contribution to mantle cooling on Venus. Venusian chasmata could have a dual character. They may be propagating rifts near major volcanic rises, and subduction trenches far from the rises in the lowlands. Subduction and rifting may occur in close proximity on Venus, unlike on Earth. Rifting induced by hotspots on Venus may be necessary to break the lithosphere and allow subduction to occur. Such a process could result in gradual lithospheric subduction or global, episodic overturn of the lithosphere.

1. INTRODUCTION

Certain segments of venusian chasmata and terrestrial subduction zone arcs share a number of morphologic, topographic, and gravimetric characteristics that suggest the possibility of terrestrial-like subduction at these sites on Venus. McKenzie *et al.* (1992) called attention to the similarities in planform curvature and asymmetric flank topography between the trenches of eastern Aphrodite Terra on Venus and the region between New Guinea and Fiji on Earth. They noted that the high trench–flank topography occurs on the concave sides of arcuate trenches on both Venus and Earth.

Sandwell and Schubert (1992a, 1992b) also pointed out that the annular moats and outer rises around large Venus coronae are similar in arcuate planform and topography to the trenches and outer rises of terrestrial subduction zones (Fig. 1). They analyzed the ridge–trench–outer rise cross-strike topographic profiles across the southeastern margins of Artemis and Latona Coronae and the northwestern rim of Eithinoha Corona in terms of the flexure of an underthrusting elastic plate and found that the flexural model could account for the venusian topographic profiles just as it does for similar terrestrial subduction zone profiles. Moreover, the flexural parameters such as plate thickness, plate curvature, and bending moment inferred from the analyses of the venusian topographic profiles were found to be comparable to the parameters derived from analyses of terrestrial subduction profiles. The South Sandwich trench (South Atlantic, Earth), the Aleutian trench (North Pacific, Earth), and the Chile trench (Southeast Pacific, Earth) are terrestrial analogues of the southern trench of Latona Corona, southern Artemis Chasma, and the northwestern trench of Eithinoha Corona, respectively, in terms of the amplitude and wavelength of the trench–outer rise topography and the flexural properties of the underthrusting plate (Sandwell and Schubert 1992a, 1992b).

Certain chasmata segments on Venus are morphologically similar to terrestrial subduction zone trenches in yet another important way. Both display normal faulting parallel to the strike of the trench on the outer trench wall and there are no cross-strike fractures across the trench. The terrestrial situation can be somewhat more compli-

0019-1035/95 $12.00

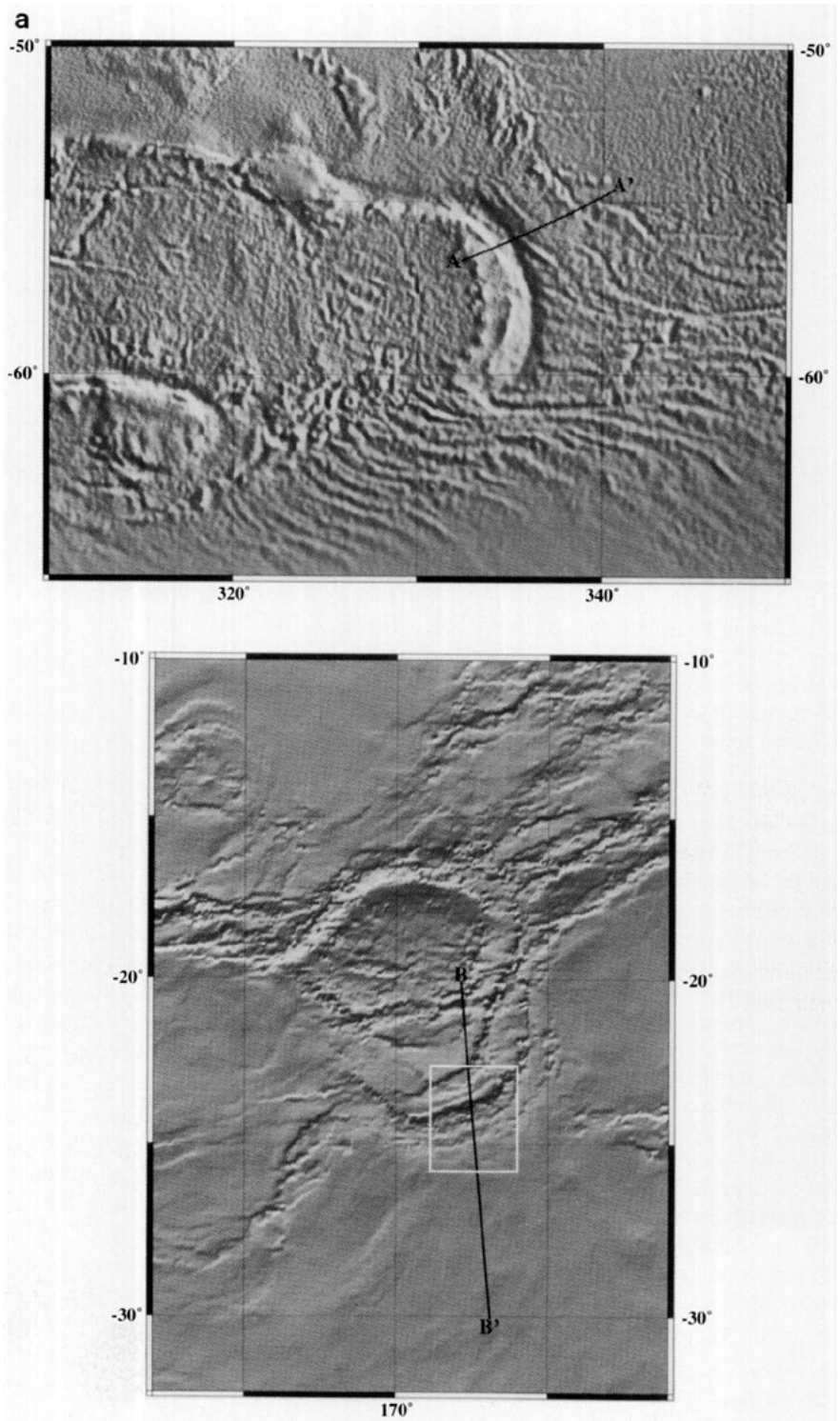

FIG. 1. (a) Seafloor topography of the South Sandwich Trench (top: South Atlantic, Earth) and the topography of Latona Corona (bottom: Venus), both illuminated from the north. A–A′ and B–B′ are the groundtracks of the topographic profiles shown in (b). These features on Earth and Venus have similar arcuate planforms consisting of an inner ridge (or ridges), a deep trench, and a broad outer rise. In the southern part of Latona Corona, a second ridge occurs inboard of the first ridge; both ridges follow the outboard arcuate trench. The topographic profiles in (b) also illustrate the ridge–trench–outer rise structure. The dashed curves in (b) are elastic flexural fits to the topographic profiles; the elastic plate thicknesses h_e associated with the fits are given in (b).

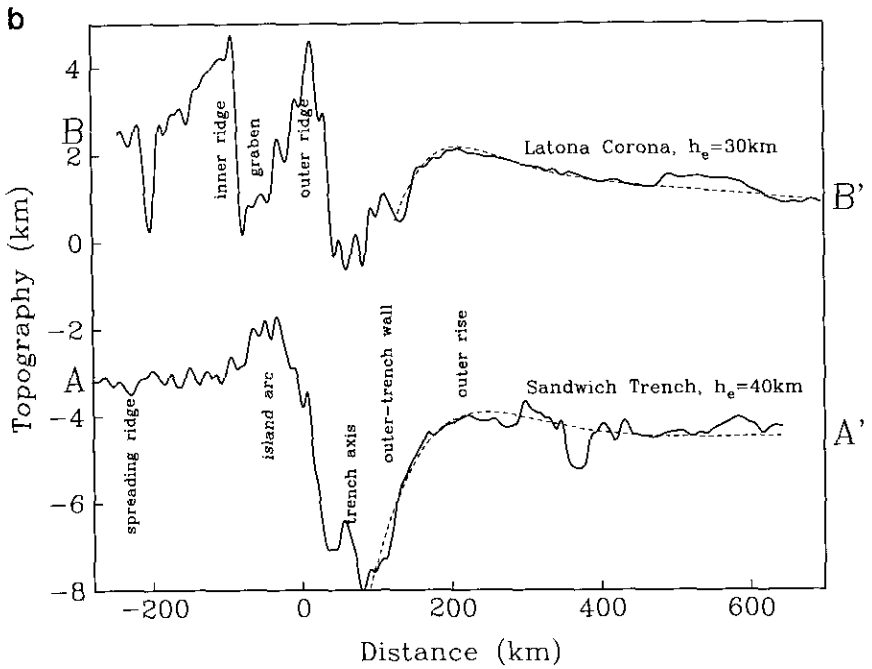

FIG. 1—*Continued*

cated because the outer-rise normal faults can be preferentially reoriented by preexisting abyssal fabric (Masson 1991). The flexural analyses of topographic profiles across the trenches of Latona Coronae and northern Eithinoha Corona show that there is generally good correlation between the locations of faults on the outer trench walls and the analytical predictions of high surface stresses due to plate flexure (Sandwell and Schubert 1992b). Faulting at these locations on Venus is consistent with the large outer rise curvatures at these sites (about 3×10^{-7} m^{-1} at northern Eithinoha and southern Latona Coronae, Sandwell and Schubert 1992a, 1992b) which indicate partial to complete failure of the lithosphere (McAdoo *et al.* 1978, McNutt 1984, McQueen and Lambeck 1989, Mueller and Phillips 1995). The southern Artemis Corona also has a very large outer rise curvature (about 10^{-6} m^{-1}, Sandwell and Schubert 1992b), but lacks extensional fractures on the outer trench wall (Suppe and Conners 1992, Brown and Grimm 1995). The large outer rise and the absence of extensional fractures may be due to a dominant in-plane compressive force (Sandwell and Schubert 1992b, Brown and Grimm 1995). Thus, the absence of extensional features does not preclude subduction at southern Artemis Corona or in general (Parsons and Molnar 1976).

Variations in the gravity field of Venus provide further support for the possibility of subduction along certain arcuate segments of chasmata (Schubert *et al.* 1994). Prominent intermediate-wavelength (600 km to several thousand kilometers) gravity anomalies occur on the concave sides of terrestrial subduction zone arcs and are known to be due in large part to the subducted slabs beneath the arcs (McAdoo 1981). There are also prominent intermediate-wavelength gravity anomalies on the concave sides of the trenches along the southeastern Artemis Corona, northern Latona Corona, and other arcuate segments of Dali, Diana, Hecate, and Parga Chasmata (Schubert *et al.* 1994). The large depths of compensation (150–200 km) and large geoid/topography ratios (30–35 m km^{-1}) at these sites, particularly at Artemis and Latona Coronae, are additional indications of deep positive mass anomalies due to subduction or underthrusting at these coronae and chasmata segments (Schubert *et al.* 1994).

The type of subduction that might be occurring along arcuate chasmata segments is retrograde subduction (Roeder 1975, Garfunkel *et al.* 1986) in which the trench migrates into the lithosphere on the convex side of the arc, thereby increasing the arc radius of curvature (Sandwell and Schubert 1992a, 1992b). The regional topographic slopes at possible subduction sites such as southern Artemis Corona and southern Latona Corona are downhill toward the convex side of the arc, consistent with the proposed direction of trench migration (Sandwell and Schubert 1992a, 1992b). The process of retrograde trench migration results in expansion of the interiors of coronae such as Artemis and Latona Coronae, an expansion that must be accommodated by extension akin to back-arc spreading. There is abundant evidence for exten-

sion in the interior of Artemis Corona, which is dominated by a complex system of troughs (Stofan *et al.* 1992). McKenzie *et al.* (1992) have identified features in the synthetic aperture radar images of the interior of Artemis Corona that are strikingly similar to GLORIA sidescan images of transform faults and abyssal hills on terrestrial spreading ridges.

The evidence discussed above for possible subduction on Venus, while substantial, is not sufficient to definitively establish the existence of venusian subduction. Other interpretations include diapiric uplift followed by gravitational relaxation (Stofan and Head 1990, Stofan *et al.* 1992, Squyres *et al.* 1992, Janes *et al.* 1992), differential thermal subsidence (Sandwell and Schubert 1992b), limited underthrusting (Suppe and Connors 1992, Brown and Grimm 1995), and rifting (Hansen and Phillips 1993). For many of the trenches that we examine below, the ridge-to-trench relief is more than 2 km. If these features formed by a relaxation process, the initial topographic step would have been much greater than 2 km. For example, to match the present topography at Eve Corona (1.5 km) would require viscous relaxation of a 300-km radius plateau having a height of 3 km (Janes *et al.* 1992), while at Heng-o Corona, about 2.5 km of thermal relaxation is required to match the present topography (~1 km). At present, there are no examples of such steps exceeding 2 km on Venus. Subduction on Earth is proved only by the wealth of evidence supporting plate tectonics, including the occurrence of deep earthquakes along Benioff–Wadati zones beneath trenches (Isacks and Barazangi 1977) and recent seismic tomographic images of descending slabs (van der Hilst *et al.* 1991, Fukao *et al.* 1992). Though the seismic data needed to substantiate subduction on Venus are not available, the evidence discussed above is sufficiently compelling to support further investigation of the possibility of subduction on Venus. Accordingly, we have undertaken in this paper a global survey of possible venusian subduction sites. In what follows we present the results of that survey and discuss its implications for the dynamic and thermal state of Venus.

2. CRITERIA FOR SELECTION AS A POSSIBLE SITE OF SUBDUCTION

Our identification of possible subduction sites on Venus is based on four criteria that typify subduction trenches on Earth.

2.1. Narrow, Deep Trenches Elongate Along Strike/Arcuate Planform

The most conspicuous characteristic of terrestrial subduction trenches is that they are long (10^3 km) and narrow (10^2 km) and are curved when viewed from above. Figure 1a illustrates these features for the Sandwich Trench in the South Atlantic Ocean. The Sandwich subduction zone is a deep arcuate trench having a planform radius of curvature of about 330 km. Inside of the trench axis lies an arcuate chain of volcanoes and islands. The trench has migrated eastward by about 1100 km during the past 36 Myr, accompanied by back-arc extension that has created the Scotia Plate. Currently, the back-arc spreading ridge is at 330° longitude. The Sandwich Trench has been identified as a terrestrial analogue for Latona Corona (Sandwell and Schubert 1992a, 1992b).

2.2. Ridge–Trench–Outer Rise Topographic Profile

A topographic profile across the strike of a terrestrial subduction zone arc shows, in the direction from the concave side to the convex side of the arc, a back-arc spreading ridge, a volcanic island arc, a deep trench, and an outer rise, as illustrated in the topographic profile across the Sandwich arc in Fig. 1b. The volcanic island arc inboard of the trench is built by subduction-related volcanism of wet rock. The outer rise is a flexural upwarp of the plate that occurs as the plate is bent downward into the mantle. The good fit of a flexural model to the trench–outer rise topography in Fig. 1b substantiates the interpretation of the outer rise as a flexural upwarp.

2.3. Large Outer Rise Curvature ($\geq 10^{-7}$ m^{-1})

The curvature of the flexural outer rise topography must be relatively large for a plate that subducts deeply into the mantle. The internal stresses that bend the plate downward are proportional to the plate curvature. Subduction requires internal stresses large enough to bend plates through substantial dip angles; such large stresses cause partial to complete failure of the plate. The curvature of the Sandwich Trench topographic profile in Fig. 1b is about 5×10^{-7} m^{-1}; subducting plates on Earth have curvatures between 10^{-7} and 10^{-6} m^{-1} (McNutt and Menard 1982, Wessel 1992, Levitt and Sandwell 1995). We have therefore set 10^{-7} m^{-1} as a minimum value of plate curvature for possible subduction on Venus. Trench–outer rise topographic profiles on Venus with smaller plate curvatures could indicate underthrusting or subduction; we therefore err on the conservative side, i.e., we underestimate the amount of possible subduction on Venus, by requiring plate curvature to exceed 10^{-7} m^{-1}.

2.4. Fractures Parallel to Strike of Trench on Outer Trench Wall and Outer Rise–No Cross-Strike Fractures across the Trench

Terrestrial subduction zones commonly show normal faulting on the outer trench wall due to tensile failure in the upper part of the downwarped plate. An example of

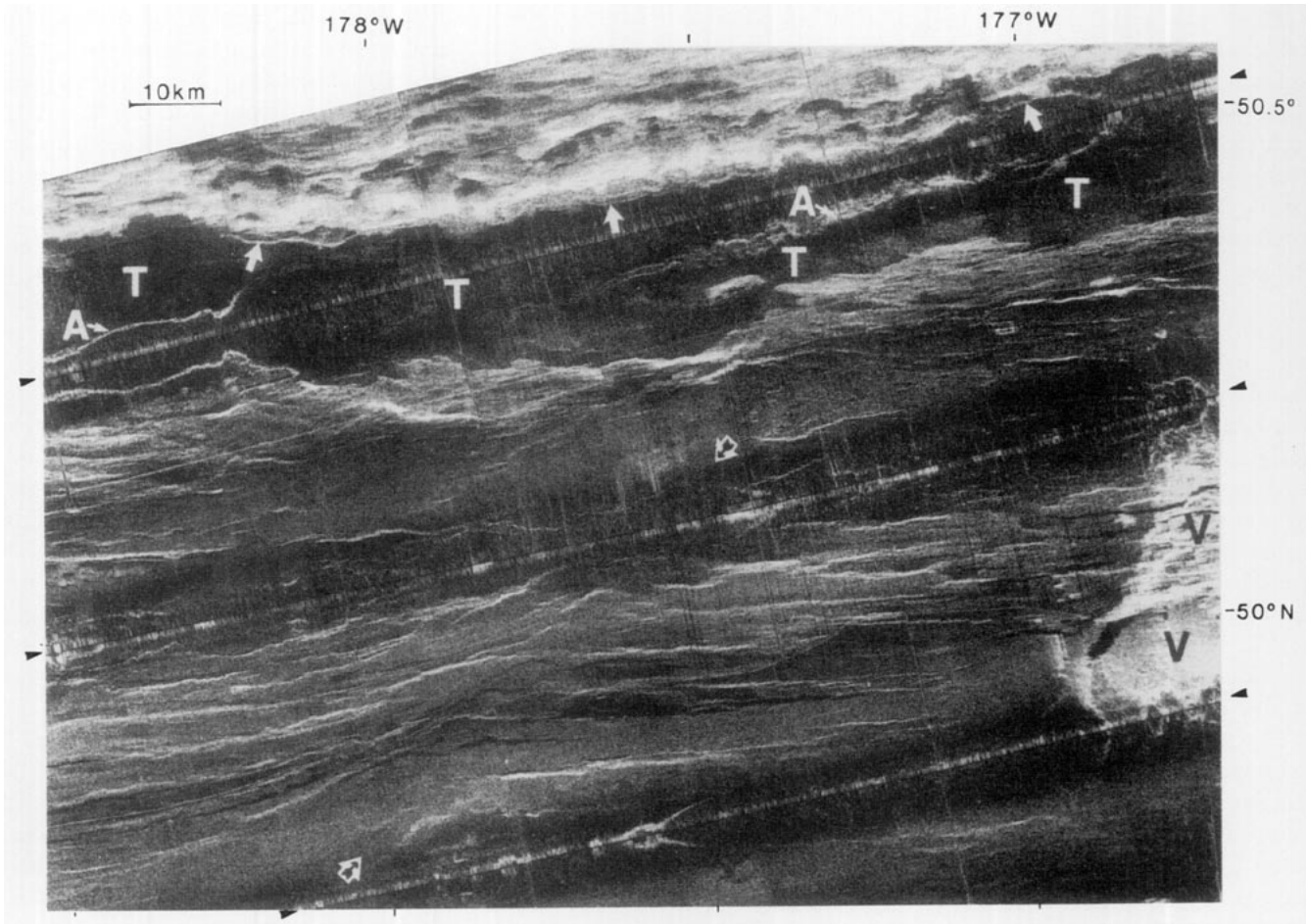

FIG. 2. GLORIA sidescan image of the Aleutian trench showing normal faulting on the outer trench wall (after Masson 1991). T, trench; A, artifact. Reprinted by permission of Kluwer Academic Publishers.

outer trench wall faulting is shown in the GLORIA sidescan image of the Aleutian trench in Fig. 2. Such faulting is generally parallel or subparallel to the strike of the trench, although an inherited oceanic spreading fabric in the subducting plate can influence the trend of the faults when there is oblique subduction (Masson 1991). The requirement that potential venusian subduction sites have outer rise and outer trench wall fractures parallel to the trench strike insures that the venusian plate has been bent downward sufficiently to cause plate failure, at least in the upper part of the plate. In some cases the fractures on the outer trench wall have been identified as compressional features (Suppe and Conners 1992). In these cases we speculate that the extensional stresses due to plate bending are overwhelmed by in-plane or near-surface compressive stresses. For all the trenches we measure the distance from the trench axis to the outermost fracture without regard to the nature of the fracture.

Fractures perpendicular to the strike of a trench and continuous across the trench from the inner trench wall to the outer trench wall would be difficult to reconcile with geologically long-term subduction. Hansen and Phillips (1993) identified some cross-strike faults in the Dali–Diana chasmata system on Venus and used them to argue against subduction on Venus. However, subduction along some segments of chasmata and coronae does not require subduction at all chasmata and coronae. In addition, extinct subduction zones could be overprinted by younger fractures that may cross the trench. We are careful to avoid identifying any chasmata segment with cross-strike fractures across the trench as a possible subduction site. Cross-strike fractures across the trench are relatively rare features in venusian chasmata.

Every possible subduction site must have a ridge–trench–outer rise topographic profile and a large outer rise curvature, but as on the Earth, some possible subduction sites may be straight or lack extensional fractures on the outer trench wall. Although we have not used it as a criterion in classifying venusian chasmata and corona segments as possible subduction sites, most but

not all of the locations we have identified as possible subduction sites have regional slopes which are downward toward the convex side of the arc. If retrograde subduction were occurring at these sites as we have proposed (Sandwell and Schubert 1992a, 1992b), then the trenches would be migrating downhill, certainly an energetically favorable direction for trench migration. Though energetically favorable, downhill trench migration is not observed on Earth.

3. LATONA CORONA

Before discussing the results of our global survey, we present the case for subduction at Latona Corona in some detail because this corona has provided the strongest evidence for subduction on Venus and we have strengthened the case since our initial proposal of subduction at Latona Corona (Sandwell and Schubert 1992a, 1992b).

Latona Corona lies within the complex Dali–Diana Chasmata system of eastern Aphrodite Terra (centered at 22° S, 172° E) (Fig. 1a). The corona is defined by two semicircular asymmetric trenches which link up on the east and west with the chasmata system and may be interpreted as oppositely directed, arcuate segments of the two chasmata. The interior of Latona Corona (about 600 km across) is not a flat plateau but instead consists of two or more topographic ridges. On average, the interior of Latona Corona lies about 1.5 km above the plains to the southeast. Figure 3 shows a detailed topography/SAR map of the southern segment of Latona Corona. The topography was derived from a SAR stereo pair (F25S174;1 and F25S174;3) using the Magellan Stereo Toolkit (Maurice and Curlander 1994). The SAR images were orthorectified using this topography and averaged to reveal the fracture patterns in relation to the major ridges, trenches, and scarps. Note the correspondence of the major circumferential fractures and major topographic steps on the outer trench wall. The stereo pair shown in Fig. 4 reveals these steps in much greater detail, as well as a major graben inboard of the trench. Take some time to view this stereo pair, especially the major structures on the north side of the images. Circumferential fractures are very intense in the deep part of the trench but decrease in intensity and frequency on the outer rise where they terminate on the crest. Impact craters are not apparent in the interior of Latona Corona, and since the interior is both elevated and highly fractured, the corona may be in a relatively early stage of thermotectonic development (Sandwell and Schubert, 1992b).

Before discussing our tectonic interpretation of these major structures, we compare topography derived from the stereo pair to altimeter profiles of topography (Fig. 5). Profiles derived from the Magellan altimetry (Fig. 5, solid curves) (Ford and Pettengill 1992) were interpolated from a 10-km spacing to a 5-km spacing so they could be compared with topographic estimates from the stereo-derived digital elevation model (Fig. 5, dashed curves). The stereo-derived elevations do not recover the mean elevation properly, and 1900 m was subtracted from the stereo topography to make it agree with the altimeter profiles. In addition, the stereo topography was shifted 4 km northward to bring it in line with the altimetry. The gaps in the dashed curves correspond to gaps in one of the two SAR images where no stereo match is possible (Fig. 3). The agreement of the altimeter and stereo topographies gives us confidence that the steep topography is reasonably well resolved by both methods. It also allows us to say that the outer rise normal faults correspond to downward steps and that the altimeter may do a good job of resolving steep scarps and troughs elsewhere on Venus, such as at the Derceto Plateau, as we discuss later.

We have previously fit flexural models to the ridge–trench–outer rise topography across southern Latona Corona and derived best fit values of the elastic parameters of the subducting or underthrusting plate (Sandwell and Schubert 1992a 1992b) (see Figs. 1b and 9h). In our model, the stationary subducting plate lies to the south of the outermost trench. In this scenario, the interior of the corona must be expanding to accommodate the trench roll-back. Here we present additional evidence for subduction and back-arc extension in the southern part of the corona.

We interpret the flat-bottom valley between the two major ridges as a graben bounded by two major normal faults (Figs. 3 and 4). The stereo-pair image (Fig. 4) shows radial fracture patterns that can be traced from the high flat area south of the southern fault all the way into the low flat area of the graben floor, suggesting that the normal fault displaced the preexisting fractures. The major southern faults are too steep to be well resolved in the stereo image. Similar fractures can be traced across the northern fault. The straightforward interpretation is that the graben formed in response to back-arc extension. The minimum amount of extension can be estimated from the average depth of the graben (~ 2 km) by assuming a fault dip. A 20° dip for each fault yields 11 km of extension while a 60° dip yields only 2.3 km of extension. Of course, the extension must be greater than this amount because not all of the extension will occur on just these two faults and after faulting, the graben floor will rebound under isostatic forces. While this amount of extension seems small compared to the overall radius of Latona Corona and is much smaller than the amount of extension at terrestrial subduction zones, the existence of these major normal faults proves that the interior of Latona Corona has expanded. The total growth of Latona Corona requires extension on many normal faults over a long period of time.

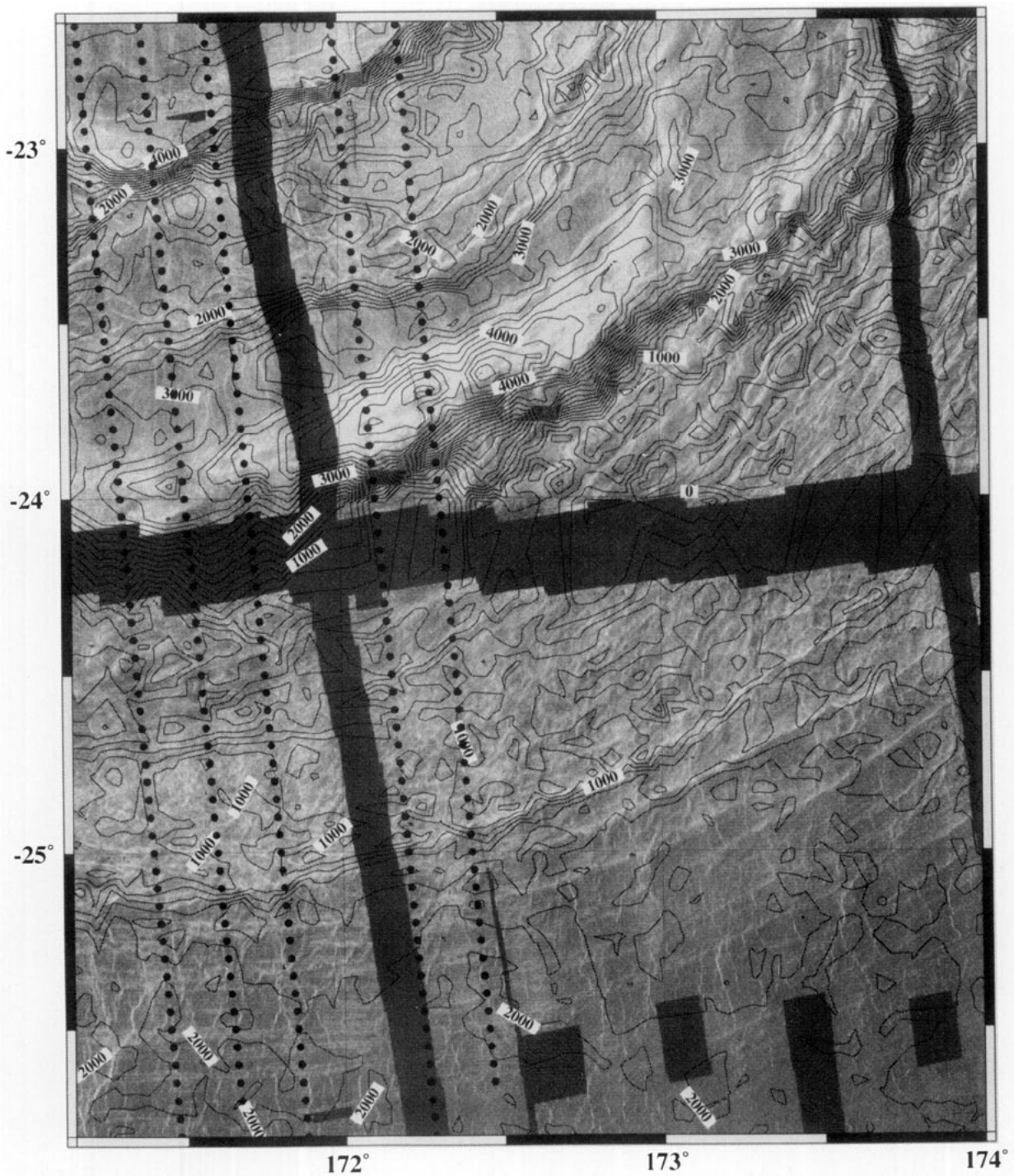

FIG. 3. Topography (200-m contour interval) of a segment of southern Latona Corona superimposed on a Magellan SAR image reveals the relationships between the circumferential fractures and the major ridges, trenches, and scarps. The major circumferential fractures correspond to the main topographic steps on the outer trench wall. The topography was generated from a stereo SAR pair (F25S174) and the SAR images were orthorectified and averaged. Black dots show tracks of five altimeter profiles of topography that are compared with the stereo-generated topography (see Fig. 5).

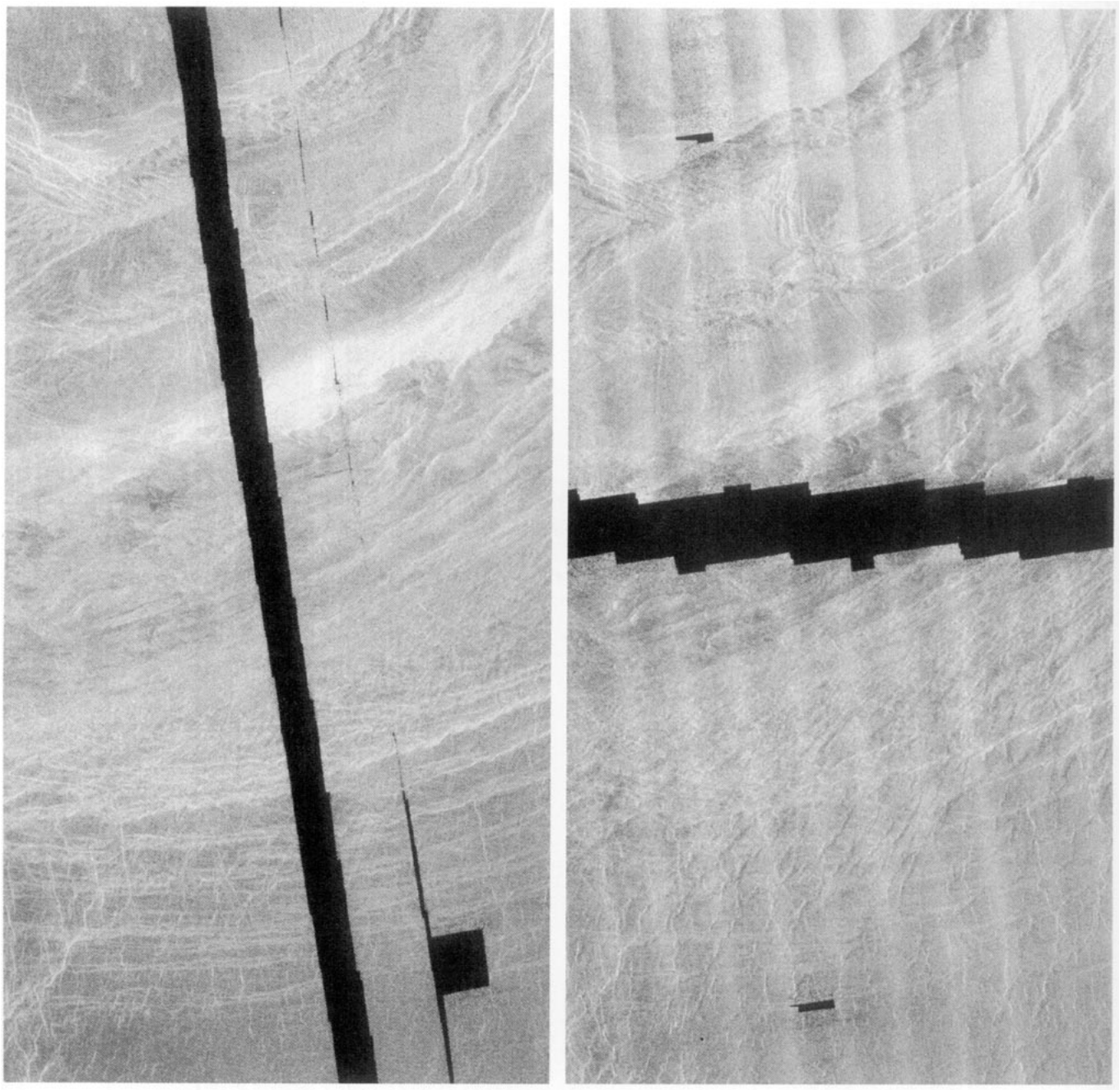

FIG. 4. Stereo pair of the segment of southern Latona Corona shown in Fig. 3. The correspondence of topographic steps and circumferential fractures on the outer trench wall is revealed in detail as well as a major graben inboard of the trench.

The flexural analysis of the trench–outer rise topography of southern Latona Corona (Sandwell and Schubert 1992a, 1992b) provides an estimate of the bending moment required to support the topographic bulge of the outer rise. We would like to determine if the maximum moment supplied by the ridges inboard of the trench is sufficient to balance the combined trench–outer rise bending moment. If the ridges are too small to maintain the trench–outer rise topography then an additional bending moment is required. The most likely source of this additional moment is a negatively buoyant subducted or underthrust slab.

Take r_0 to be the first zero-crossing outboard of the trench axis (large black dot in Fig. 6). Assume that the trench and outer rise topography are maintained by fiber stresses within a plate and that the in-plane force is zero;

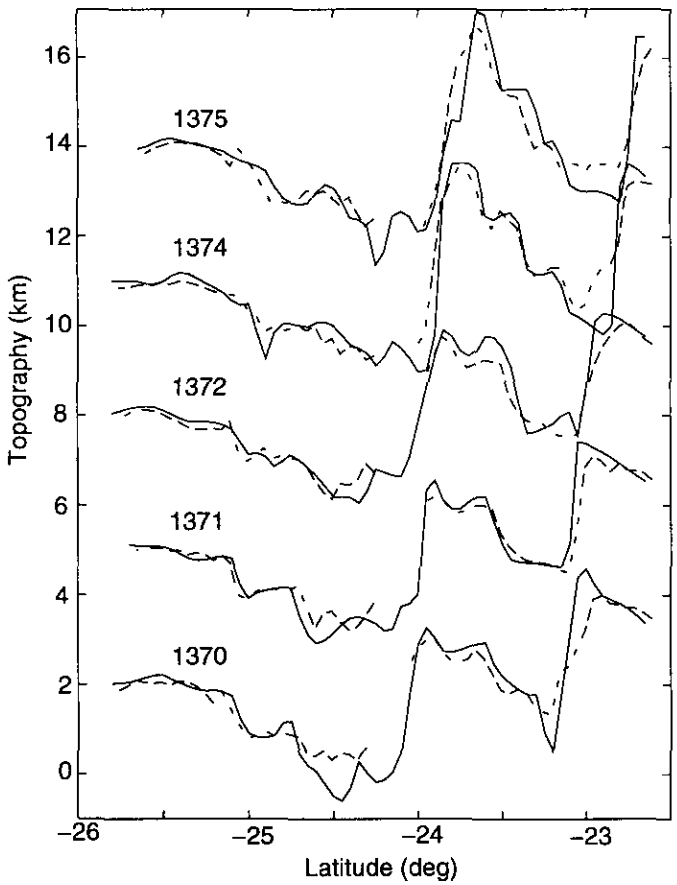

FIG. 5. Topographic profiles across the southern segment of Latona Corona shown in Fig. 3. Solid curves, profiles derived from Magellan altimetry (Ford and Pettengill 1992). Dashed curves, profiles derived from stereo digital elevation model. The gaps in the dashed curves correspond to gaps in one of the two SAR images where no stereo match is possible (Fig. 3). The altimeter and stereo topographies are generally in good agreement. Neither method resolved the steep topography of the normal faults surrounding the graben.

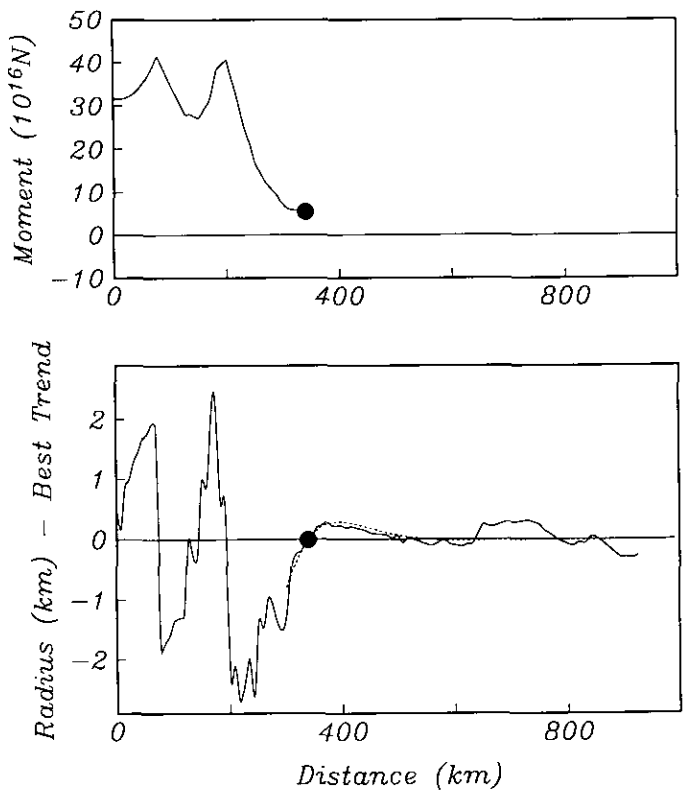

FIG. 6. Topography and bending moment exerted by the topography along orbit number 1376 crossing southern Latona Corona. The lower panel shows the topography relative to the linear slope of the best-fitting flexure model. The large black dot in the lower panel is the location of the first zero-crossing outboard of the trench axis of the best-fitting flexure model. The upper panel shows the bending moment M_s calculated according to Eq. (1). The large black dot in the upper panel is the moment of the outer rise (second term on the right side of Eq. (1)) calculated from the best-fitting flexure model. The increase in moment inboard of the zero-crossing is due to the trench, while the decreases in the moment are due to the ridges. A residual moment of about 32 × 10^{16}N (at zero distance) needed to support the outer rise must be provided by an underthrust or subducted slab.

no rheological assumption is needed (Kirby 1983). Assume further that the ridges inboard of the trench are uncompensated. Note that if they are partially compensated for by thickened crust then they will supply a smaller combined moment. Finally, assume that the linear slope of the best-fitting flexure model defines the isostatic level in the region of Latona Corona and that this level can be extrapolated inboard of the trench axis. (This is a major assumption and the moment calculations are sensitive to the slope used.) Given these assumptions, and a radius r_0 of Latona Corona of 330 km, the moment that must be supplied by the subducting slab M_s is

$$M_s = g\rho_m \int_0^{r_0} w(r)(r - r_0)\frac{r}{r_0}\,dr + g\rho_m \int_{r_0}^{\infty} w(r)(r - r_0)\frac{r}{r_0}\,dr, \quad (1)$$

where g is the acceleration of gravity, ρ_m is the mantle density, $w(r)$ is the topography with respect to a regional trend, and r is radial distance from the center of the corona. Values of parameters are given in Table III.

The calculation for orbit number 1376 crossing southern Latona Corona is shown in Fig. 6. The moment of the outer rise (second term on the right side of Eq. (1)) was calculated from the best-fitting flexure model because the flexure fit provides a smooth curve that is easily integrated. Note that this moment could also be calculated by a direct integration of the residual topography (i.e., no flexure assumption). Starting with this value at r_0 we integrated into the interior of Latona Corona to a radius of zero. The rapid increase in moment inboard of r_0 is due to the trench while the major ridges decrease the integrated moment. Even the inclusion of the moment due

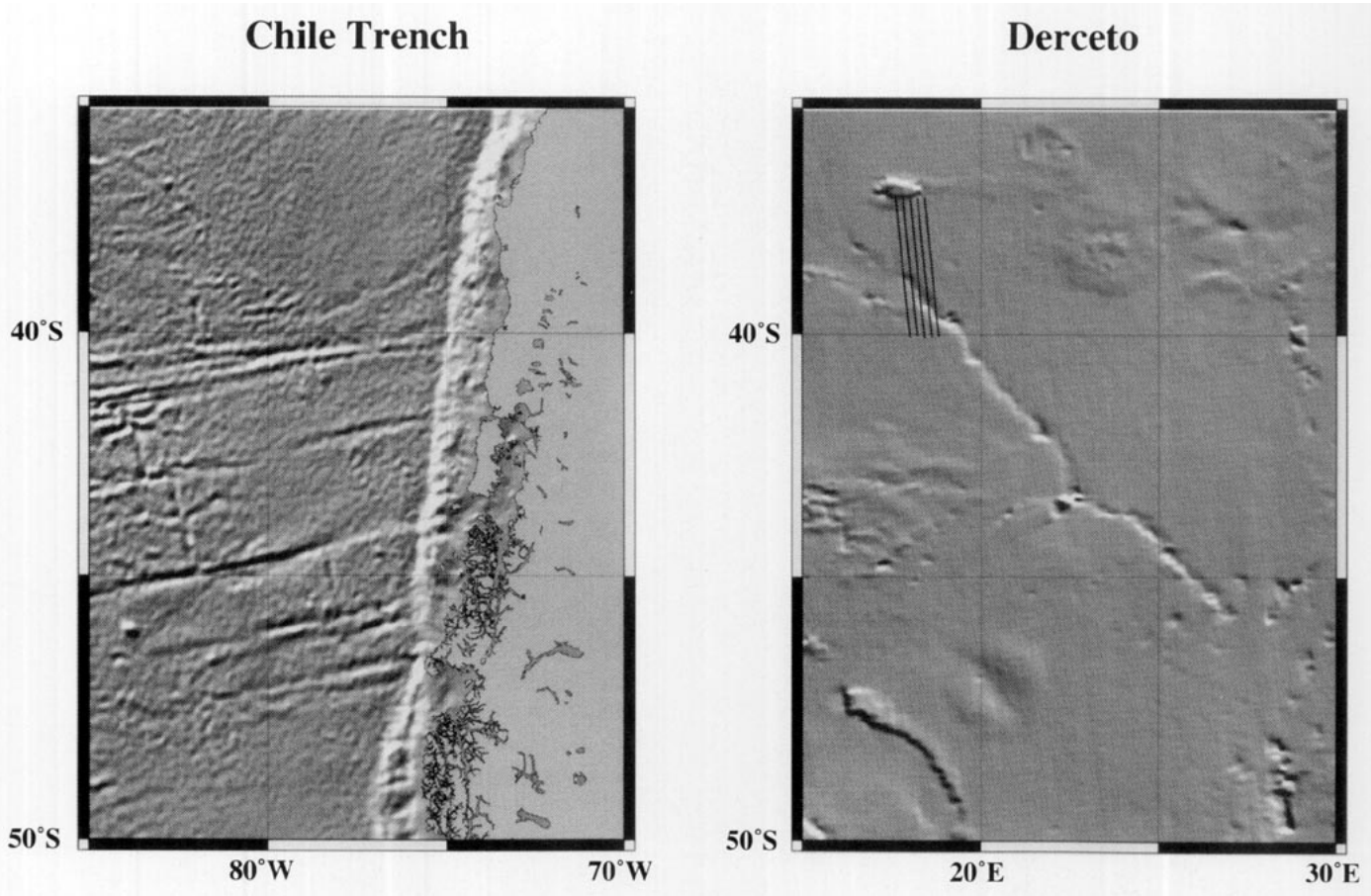

FIG. 7. Topography of the Chile Trench, Earth (left) and the Derceto Plateau, Venus (right) illuminated from north. Subduction of a very young and thin plate is taking place at the Chile Trench as can be seen by the ridge segments offset by fracture zones in close proximity to the trench. The trench along the eastern margin of Derceto Plateau may be a site of subduction of relatively thin lithosphere as at the Chile Trench. The lines crossing the trench on the eastern boundary of Derceto Plateau are the groundtracks of topographic profiles shown in Fig. 9b. Topography along these groundtracks shows the ridge–trench–outer rise signature typical of terrestrial subduction zones.

to the second ridge inboard of the trench is not sufficient to supply the flexural moment of the trench and outer rise. The missing moment is very large, about 32×10^{16} N or five times greater than the moment needed to support the outer rise. Most of the required moment is related to the extreme depth and width of the trench at Latona Corona. One could vary the regional trend or use a curved regional model to reduce the moment but it is impossible to reduce it to zero unless an extreme regional model is used.

Previously, we estimated M_s assuming a two-dimensional trench (i.e., infinite r_0) (Sandwell and Schubert 1992a) and found that the topography inboard of the trench could supply the required trench and outer rise bending moment ($M_s \approx 0$), but only when the second inboard ridge was included. Since this second ridge is more than half a flexural wavelength (i.e., width of outer rise) away from the trench it is unlikely to contribute to the moment balance. The more appropriate cylindrical geometry used here suggests that a subducted or underthrust slab is required to support the outer rise at southern Latona Corona.

We also performed a similar calculation at the south Sandwich Trench on Earth and found that the topography inboard of the trench was sufficient to maintain the moment of the trench and outer rise. However, on Earth, the topography of the volcanic arc inboard of a trench is largely balanced by the upward buoyancy of its thick crustal root and so it does not exert a major downward force on the subducted slab. Thus on Earth one cannot prove that a negatively buoyant subducted slab exists based on these moment calculations; deep earthquakes along a Benioff zone provide the definitive evidence for subduction at the Sandwich Trench.

4. DERCETO PLATEAU

An example of a possible subduction site on Venus quite different from Latona Corona is the eastern margin

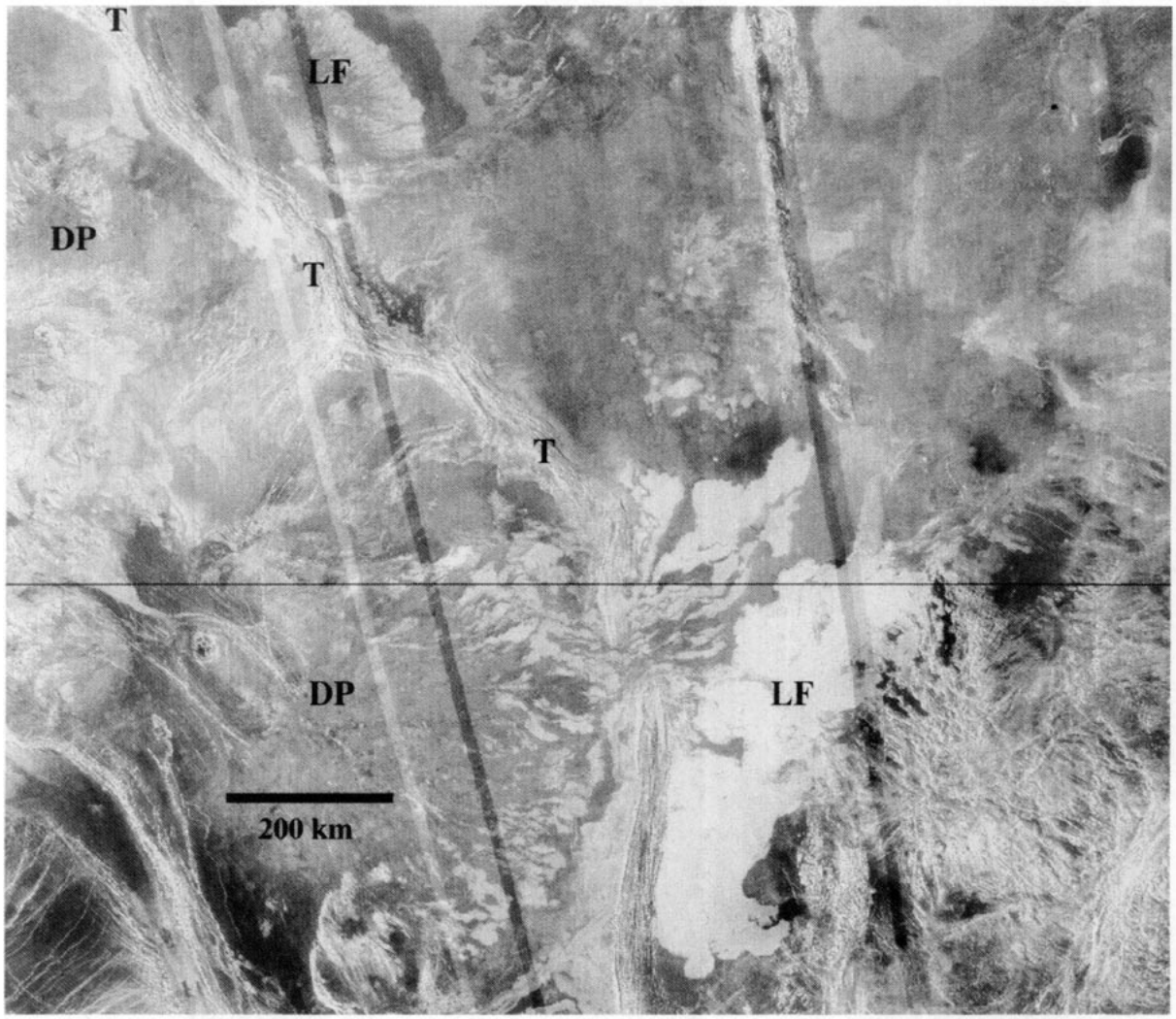

FIG. 8. Magellan SAR image of eastern Derceto Plateau (DP). The eastern boundary of the plateau is bounded by a trench with prominent trench-aligned fractures all along its length (T). A lava flow (LF) (lower center of image) flows eastward (downhill) from Derceto Corona, buries the trench, and flows out onto the plains. Another lava flow (upper left) flowed eastward from the interior of the plateau onto the plains, but this flow is cut by the younger trench and its outer-trench-wall fractures.

of the Derceto Plateau. The region we refer to as the Derceto Plateau is an oval-shaped volcanic plateau elongated to the northwest and elevated by a few hundred meters above the surrounding plains (Fig. 7) (Baer *et al.* 1994). It is about 1600 km long and 600 km wide and is located at the intersection of two major extensional belts, the northwest trending Alpha–Lada belt and the north-northeast trending Derceto–Quetzalpetlatl belt. The Alpha–Lada extensional belt is over 6000 km long and 50–200 km wide and includes the coronae Eve, Tamfana, Carpo, Selu, Derceto, and Otygen. The Derceto–Quetzalpetlatl belt is about 2000 km long and 300 km wide in places and includes the coronae Sarpanitum, Eithinoha, and Quetzalpetlatl (Baer *et al.* 1994). The Derceto Plateau is named for Derceto Corona, which is the major center of volcanism on the plateau.

The plateau is surrounded by zones of intensive deformation which take the form of an arcuate system of ridges and trenches on the eastern margin of the plateau (Baer *et al.* 1994) (Fig. 8). We interpret a segment of the eastern margin of Derceto Plateau as a possible subduction site and show in Fig. 9b topographic profiles of the ridge–trench–outer rise signature along the ground tracks over this segment in Fig. 7. The dashed curves in Fig. 9b are flexural model fits to the topography. The depth of the trench along this segment is between about 500 m and 1 km and the amplitude of the outer rise is usually less than 100 m. The elastic thickness of the subducting plate at Derceto Plateau and other parameters inferred from these flexural fits are given in Table I. The elastic thickness of the plate is only 6 km, by far the thinnest of all the potential subducting plates listed in the table. The

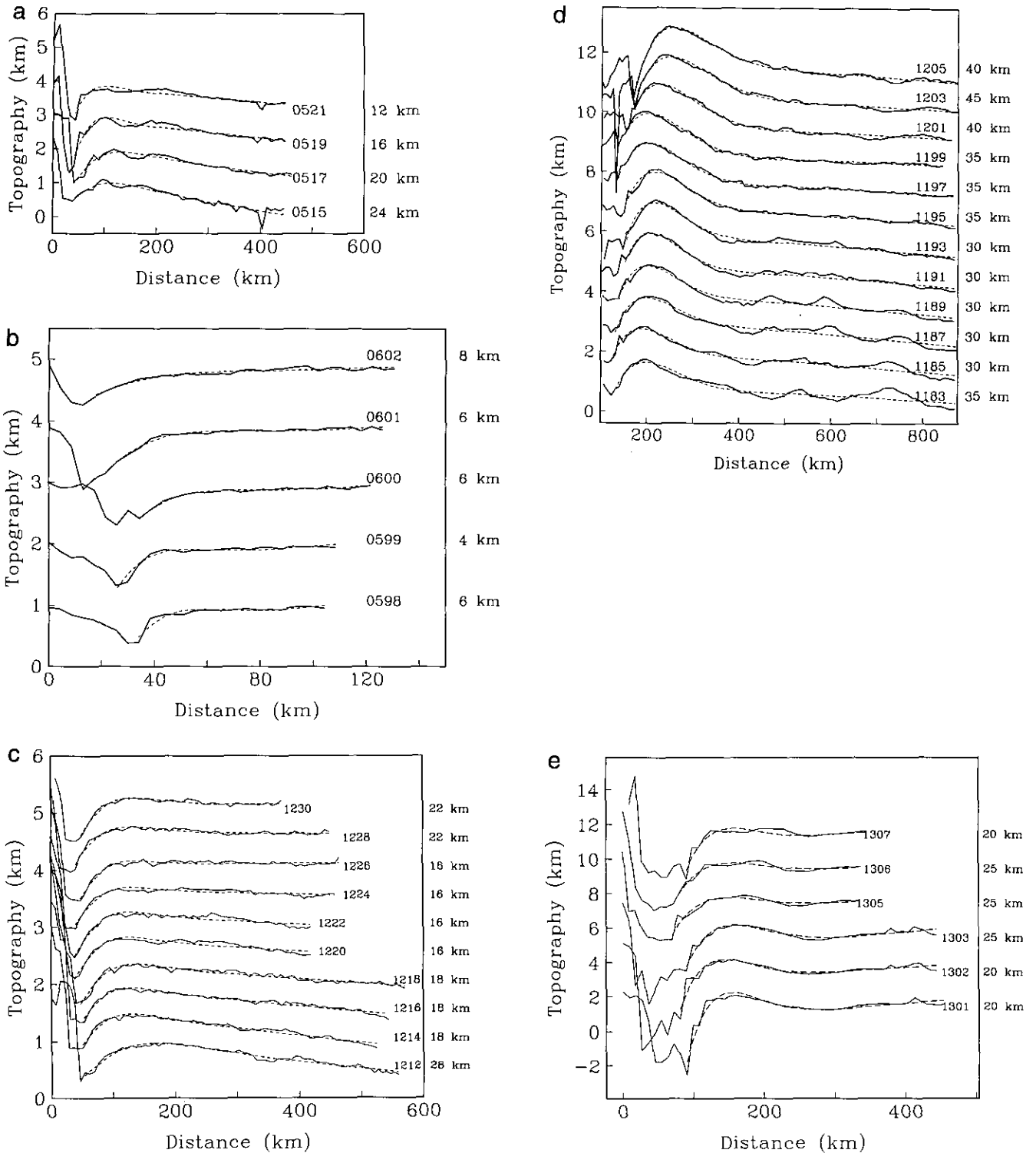

FIG. 9. Ridge–trench–outer rise topographic profiles across the potential sites of subduction shown in Fig. 10 and listed in Table I. (a) Eithinoha Corona, (b) Derceto Plateau, (c) Nightingale Corona, (d) Artemis Corona, (e) East Diana Chasma, (f) western Dali Chasma, (g) northern Latona Corona, (h) southern Latona Corona, (i) Neyterkob Corona, (j) Hecate Chasma, (k) Parga Chasma, (l) northern Demeter Corona, (m) South Demeter Corona, (n) Uorsar Rupes, and (o) Quetzalpetlatl Corona. The dashed curves are the best flexural model fits to the trench–outer rise topography. Magellan orbit numbers are listed adjacent to the profiles as are the elastic plate thicknesses of the flexural model fits.

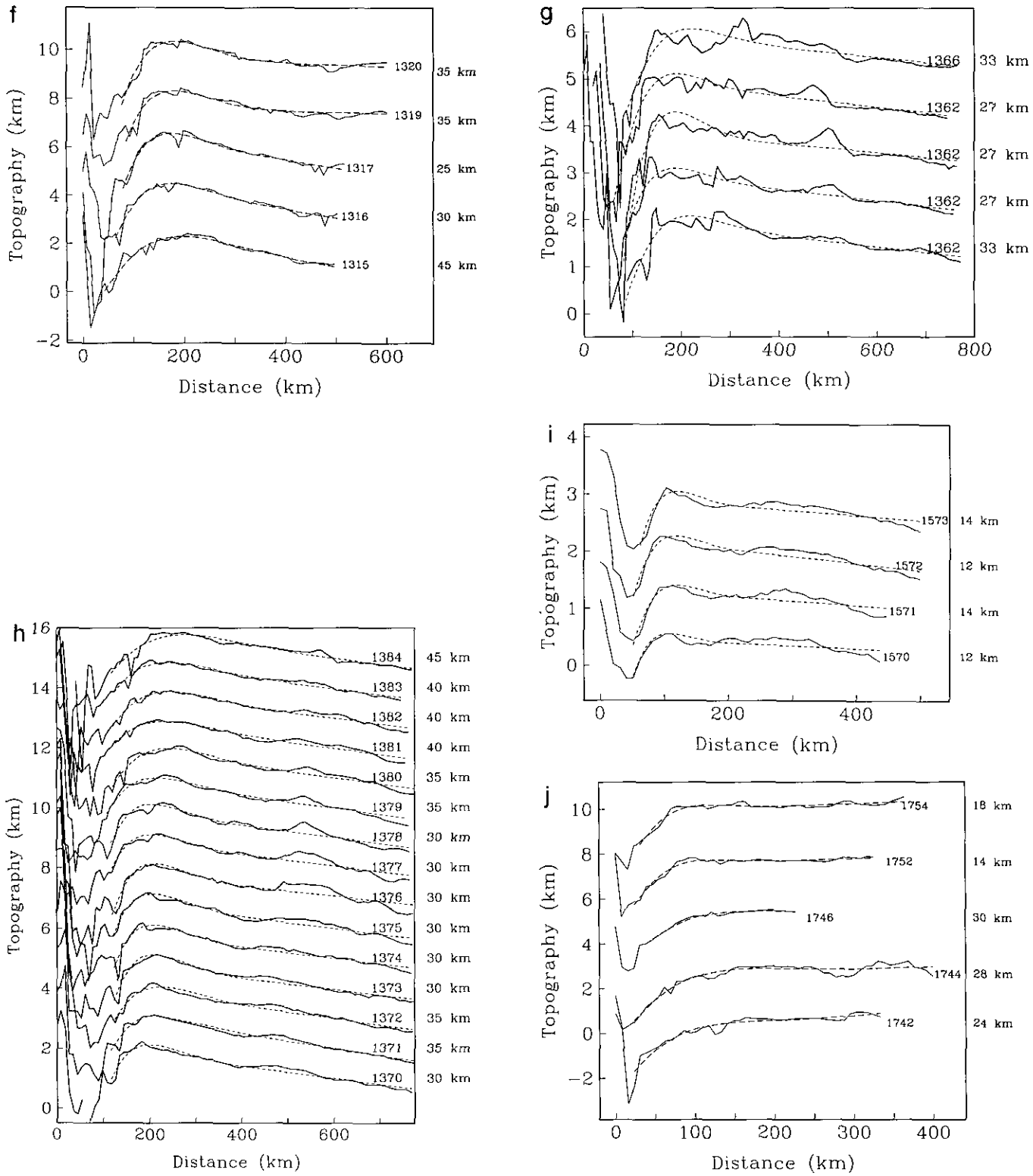

FIG. 9—*Continued*

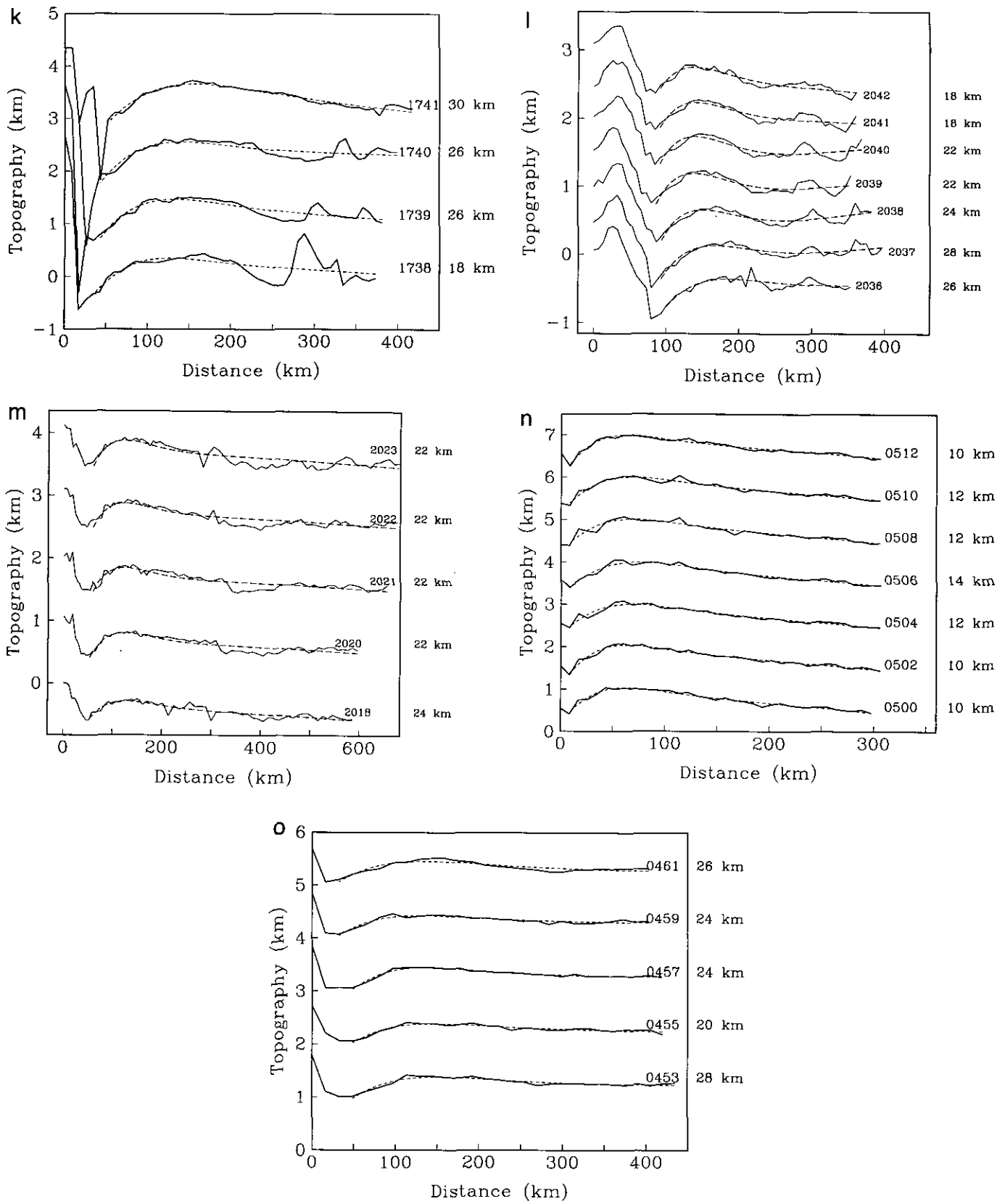

FIG. 9—*Continued*

TABLE I
Subduction and Overthrust Features

	Feature	Lat. (deg.)	Long. (deg.)	Subduction Zone Length[a] (km)	Candidate Subduction Zone Length[b] (km)	Elastic Thickness (km)	Regional Slope 10^{-3}	Regional Elevation 6051.9 km	Plate Bending Moment (10^{16} N)	Plate Bending Curvature (10^{-7} m^{-1})	Planform Radius (km)	Distance of Fractures from Trench(km)	Magellan Image ID#†
1	Eithinoha Corona	−58.1	8.3	465	429	18.0	−1.9	0.14	1.0	3.3	230	90	C60S014
2	Derceto Plateau	−47.6	19.7	1759	641	6.0	3.6	−0.35	0.2	209.4	–	< 10	C45S032
3	Nightingale Corona	61.7	130.2	0	592	19.0	−0.6	0.06	0.7	1.6	220	–	F60N132
4	Artemis Corona	−37.4	135.0	1913	1658	34.6	−1.1	0.21	25.4	10.3	1300	80	C45S138
5	E. Diana Chasma	−15.6	157.2	1109	450	22.5	2.9	−0.32	12.4	19.9	–	70	C15S163
	W. Dali Chasma					34.3	−2.1	1.42	12.9	5.7	–	140	C15S163
6	N. Latona Corona	−20.4	171.4	1389	0	29.4	−1.2	1.21	4.7	34.5	330	> 150	F15S159
	S. Latona Corona					34.3	−2.1	1.33	6.4	3.1	330	170	F25S174
7	Neyterkob Corona	48.9	204.8	178	239	13.5	−0.9	−0.32	0.8	5.9	120	80	F50N205
8	Hecate Chasma	16.5	248.4	611	311	22.8	1.5	−0.93	2.4	3.7	–	130	C15N249
9	Parga Chasma	−15.4	245.4	388	367	25.0	−1.0	−0.34	1.6	17.2	90	–	C15S249
10	N. Demeter Corona	54.4	295.1	240	698	22.6	0.3	−1.49	3.1	4.6	> 180	50	C60N291
	S. Demeter Corona					22.4	−0.5	−1.12	2.0	3.2	> 180	25	C60N291
11	Uorsar Rupes	77.8	331.2	299	666	11.4	−2.1	0.20	0.28	33.2	> 400	–	C75N338
12	Quetzalpetlatl Corona	−66.6	350.0	611	338	24.4	−0.4	0.51	0.85	9.8	550	65	C60S347
	TOTAL			8962	6388								

[a] White in Fig. 10.
[b] Black in Fig. 10.
† F stands for FMIDR, C stands for C1MIDR, MIDR (merged image data record).

outer rise curvature, 2.1×10^{-5} m^{-1}, is also the largest, by a factor of 6, of all the curvatures reported in Table I. The Derceto Trench is the straightest of all the long trench segments listed as possible subduction trenches. It is also one of the few trenches at which the direction of retrograde migration is not downhill. A terrestrial analogue of the Derceto Trench may be the Chile Trench (Fig. 7). The subducting plate is very thin at the Chile Trench due to subduction of the Chile Rise at this trench (Fig. 7).

At 47° S along the Derceto Trench there is an example of a lava flow that originated in Derceto Corona and flowed eastward, burying the trench and flowing out onto the surrounding plains (Fig. 8). At 41° S there is another lava flow that flowed out from the corona to the east onto the plains, but in this case the trench and its fractures, interpreted by Suppe and Conners (1992) as compressional and due to overthrusting, cut the lava flow, indicating that the trench is younger than the flow. These features may illustrate the growth and expansion of the Derceto Plateau. Lava flows from the interior of the plateau to the exterior, filling the trench and spreading out onto the plains; the interior expands, recreating the trench and flexing the outer plate.

5. QUETZALPETLATL CORONA

Quetzalpetlatl Corona is the southernmost corona along the north-northeast trending extensional belt ending at Derceto Corona and it was the first corona to be partially imaged by Magellan (Solomon *et al.* 1991). Quetzalpetlatl Corona is about 800 km in diameter; it is elongate along the north-northeast direction and on average is about 1 km above its surroundings (Solomon *et al.* 1991; Baer *et al.* 1994). Along the northwestern margin of Quetzalpetlatl Corona there is an annulus of ridged terrain just inboard of a trench partially filled with lava. The topography of the northwestern margin of Quetzalpetlatl Corona displays the ridge–trench–outer rise signature typical of terrestrial subduction zones; this margin of Quetzalpetlatl Corona also satisfies all of the criteria set out earlier for classification as a possible site of subduction on Venus and accordingly we identify it as a possible subduction zone.

Topographic profiles across the northwestern margin of Quetzalpetlatl Corona are shown in Fig. 9o. The volcanically flooded trench is only several hundred meters deep and the outer rise has an amplitude of only about 100 m. Flexural fits to these topographic profiles (dashed curves in Fig. 9o) yield estimates of the elastic thickness of the lithosphere outboard of the moat ranging from 20 to 28 km (Fig. 9o). Though the trench and outer rise have low amplitudes, the outer rise curvature is nearly 10×10^{-7} m^{-1} and the relatively large elastic thickness of the plate requires a moment of nearly 10^{16} N to accomplish the bending (Table I). Because the trench has been filled with lava that likely originated from fractures in the vicinity of the annulus, the actual trench is certainly deeper and the plate has surely undergone more bending than is apparent in the present topography.

The northwest margin of Quetzalpetlatl Corona is the only place around the corona with a clear expression of

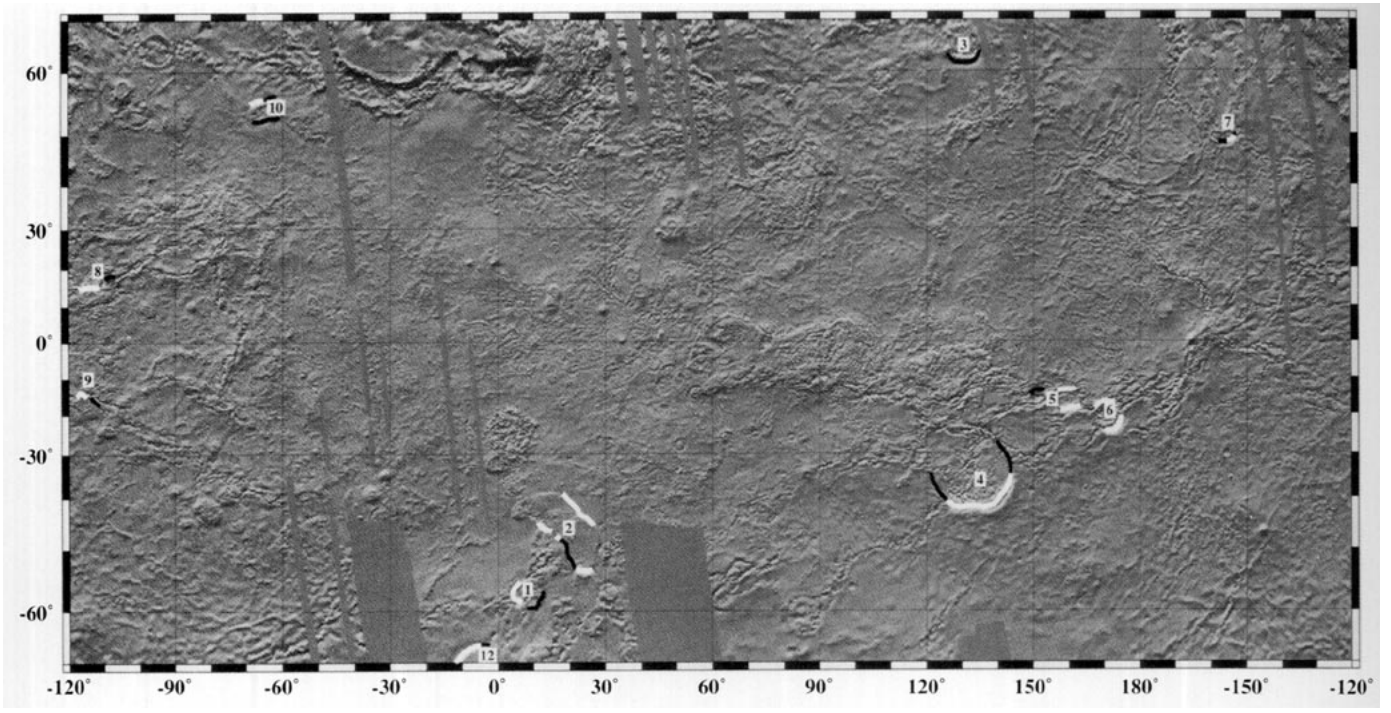

FIG. 10. Topographic map of Venus (illuminated from the north) showing possible subduction zones (trench segments satisfying most of the criteria listed earlier, white arcs) and candidate subduction zones (trench segments satisfying some of the criteria for subduction, black arcs). Characteristics of the potential subduction zone sites are summarized in Table I and listed according to the numbers shown in the figure. The site at Uorsar Rupes (11) is too far north to be shown on the map.

ridge–trench–outer rise topography. The northeast part of the corona is dominated by a bulge elevated about 1 km above the average height of the corona. The bulge extends over 200 km northeast of the corona and is extensively deformed by northeast-trending grabens and fractures (Solomon *et al.* 1991; Baer *et al.* 1994). The southern part of Quetzalpetlatl Corona is covered by volcanic flows and there is no evidence of an annular ridge and trench.

6. A SUMMARY OF POTENTIAL SITES OF SUBDUCTION ON VENUS

We have identified a total of a dozen locations as potential sites of subduction on Venus (Table I and Fig. 10). Of these, the sites at Uorsar Rupes (Solomon and Head 1990), Eithinoha, Artemis, and southern Latona Coronae have already been identified as possible subduction zones (Sandwell and Schubert 1992a, 1992b). The other potential subduction sites are identified by us here for the first time and include the Derceto Plateau, Nightingale, northern Latona, Neyterkob, Demeter, and Quetzelpetlatl Coronae, and eastern Diana, western Dali, Hecate, and Parga Chasmata. The trench–outer rise topographic profiles and flexural fits used to determine the elastic thicknesses, curvatures, and bending moments of all the sites listed in Table I are shown in Figs. 9a–9o. The SAR images (i.e., FMIDR or CMIDR) associated with the trench profiles are listed in Table I. Topographic profiles and flexural fits for the sites at Nightingale, Nyterkob, and Demeter Coronae and western Dali Chasma have been discussed in Johnson and Sandwell (1994).

The potential subduction zone sites that satisfy most of the criteria given earlier are listed in Table I and located on the map of Fig. 10 as white trench segments. (Numbers in the table correspond to those in the figure. Feature 11, Uorsar Rupes, is at too high a northern latitude to be shown on the map.) The table gives the length of the trench segment associated with each subduction feature. In only one case, Nightingale Corona, is a trench length of 0 km recorded. The trench segment of Nightingale Corona is colored black, as are other trench segments in Fig. 10, indicating that one of the two required criteria for classification as a potential subduction site is not satisfied. Either the ridge–trench–outer rise expression was not clear or the plate curvature was less than about 10^{-7} m^{-1} (Nightingale Corona). Nevertheless, we have located such trench segments on the map as strong candidates for subduction zones and list their lengths in Table I under the column labeled "candidate subduction zone length."

At each of the sites in Table I the reported value of elastic thickness is the average of the values that minimize the rms misfits between flexural and actual topographic

TABLE II
Flexural Properties of Subduction Trenches on Earth

Trench	Elastic Thickness (km)	Plate Bending Curvature (10^{-7} m^{-1})	Plate Bending Moment (10^{16}N)
Middle America	12	5.8	0.6
Chile	20	7.0	3.2
Aleutian	30	5.0	7.8
Peru	40	2.6	9.4
Sandwich	40	4.9	18.3
Izu-Bonin	40	4.9	18.4
Kuril	45	4.2	22.5

profiles. Moments, curvatures, regional slopes, and regional elevations given in the table are also averages of the modeled profiles. The table also includes the planform radius of the trench and the distance of fractures from the trench. To help in understanding the significance of the results in Table I, we summarize the relevant characteristics of some terrestrial trenches in Table II (Sandwell and Schubert 1992a).

7. DISCUSSION OF RESULTS

The total length of possible subduction trenches on Venus is about 9000 km (Table I); if the candidate subduction trenches (those identified in black in Fig. 10) are added, the total subduction zone length on Venus is over 15,000 km. This is to be compared with 37,000 km of subduction trenches on Earth (Reymer and Schubert 1984). The length of subduction zones on Venus is possibly 25% of the length of subduction zones on Earth and might be as large as 40% or more. The longest potential subduction zone on Venus is Artemis Corona, with the Derceto Trench a close second. The possible subduction trenches at the Latona Corona and Dali–Diana Chasmata sites are also quite long, each being well in excess of 1000 km in length. These sites alone constitute nearly 70% of the 9000 km of possible venusian subduction zones.

Elastic thicknesses of possible subducting plates on Venus range from about 6 km (Derceto Plateau) to about 35 km (Artemis and southern Latona Coronae and western Dali Chasma); subducting plates on Earth have elastic thicknesses that vary over a similar range (15–50 km) (Table II and Levitt and Sandwell 1995). Elastic thicknesses of terrestrial plates depend on their ages at subduction: the older the plate the larger the elastic thickness (Caldwell and Turcotte 1979). It is not known, of course, if a similar age dependence of elastic plate thickness applies to Venus as well. Though the range of elastic plate thicknesses on Venus is relatively large, 8 of the 12 sites in Table I have elastic plate thicknesses between 18 and 25 km.

Plate curvature at venusian subduction sites (not including Nightingale Corona) varies from about 3×10^{-7} m^{-1} at Latona and Eithinoha Coronae to the very large value of about 2×10^{-5} m^{-1} for the very thin plate at the eastern margin of Derceto Plateau. Aside from the Derceto Plateau, the largest plate curvatures in Table I are about 35×10^{-7} m^{-1} at northern Latona Corona and Uorsar Rupes. On Earth, the curvatures of subducting plates vary between about 3×10^{-7} and 10^{-6} m^{-1} (Table II). Bending moments of possible subducting plates on Venus lie between about 0.2×10^{16} N (Derceto Plateau) and 25×10^{16} N (Artemis Corona); bending moments of subducting terrestrial plates span the same range of values. Only the sites at Artemis, eastern Diana, and western Dali Chasmata have bending moments in excess of 10×10^{16} N. The bending moments at Latona Corona are about 5×10^{16} N. Bending moments are $O(10^{16}$ N) or smaller at all other sites.

The similarity in the elastic properties, e.g., elastic plate thickness, of subducting plates on Venus and Earth despite the high surface temperature of Venus is likely due to the extreme dryness of the venusian environment. The importance of the lack of water in stiffening rocks has been demonstrated in recent experiments on the creep properties of very dry diabase (Mackwell *et al.* 1995).

8. THERMAL AND DYNAMICAL IMPLICATIONS

8.1. Heat Transfer

The effectiveness of plate subduction as a heat transfer mechanism in Venus depends not only on the total length of subduction trenches on Venus but also on the rate of trench rollback and the variation of these parameters through geologic time. On Earth, plate subduction is the main mechanism for cooling the mantle. Since we do not know the rate of trench migration on Venus we cannot adequately assess the contribution of plate subduction to cooling the planet. However, based solely on cumulative trench length on Venus, mantle cooling by plate subduction, *though less effective than on Earth, may still be* significant.

Turcotte (1993, 1995) has argued that neither plate subduction, hotspot volcanism, nor conductive cooling through the lithosphere could maintain Venus in a quasi-steady heat balance with its internal radiogenic heat production. Instead, he has proposed that heat transfer in Venus is episodic and occurs by the sudden massive overturn of lithosphere that has cooled and thickened through time until it becomes gravitationally unstable. Heat is trapped within the mantle prior to the overturn and is released during the event. The last such overturn is hypothesized to have occurred about 500 million years ago, in accordance with one model of the venusian cratering

record (Schaber *et al.* 1992). Some of the subduction trenches we have identified could be remnants of the last overturn while others could mark the beginning of the next event.

From a fluid dynamic point of view, an internally heated planet like Venus must cool by a lithospheric foundering process such as subduction or delamination. The only question is the temporal nature of the process, i.e., whether it is gradual or episodic. Since we have identified subduction trenches on Venus whose lengths total a substantial fraction of the trench length on Earth, the lithospheric foundering process on Venus might occur by retrograde trench migration in a much more gradual way than envisioned by Turcotte (1993, 1995) especially if Venus is currently in a period of reduced subduction activity or we have underestimated the length of trenches on Venus by the conservatism of our classification scheme.

8.2. *Lithospheric Buoyancy*

It has been argued by some (e.g., Burt and Head 1992, Phillips and Malin 1983) that the lithosphere of Venus would be too light to subduct. However, these analyses assumed a higher lithospheric temperature gradient than is suggested by the more recent estimates of elastic plate thickness (Sandwell and Schubert 1992a, 1992b, Johnson and Sandwell 1994, Solomon *et al.* 1994, Phillips 1994). A simple calculation below shows that the lithosphere of Venus is subductible given sufficient time for the lithosphere to cool and thicken and accumulate enough negative buoyancy to offset the positive buoyancy of the crust. Lithospheric buoyancy can be quantified by the introduction of a density defect thickness δ, defined by (Oxburgh and Parmentier 1977)

$$\delta = \int_0^\infty \left[\frac{\rho_m - \rho(z)}{\rho_m}\right] dz, \tag{2}$$

where $\rho(z)$ is the lithospheric density, z is depth in the lithosphere, and ρ_m is the undepleted mantle density. The integration extends over the entire thickness of the lithosphere which, for mathematically suitable representations of $\rho(z)$, can range from zero to infinity (Turcotte and Schubert 1982). The lithosphere is stable for positive δ and unstable for negative δ. Contributions to δ come from the combined crust–mantle density difference and the density difference due to mantle depletion δ_{comp}, and the thermally induced density difference between the cold lithosphere and hot underlying mantle $\delta_{thermal}$. The compositional density difference depends only on crustal thickness (we use the value of δ_{comp} from Oxburgh and Parmentier (1977) for an oceanic crustal thickness of 8 km and scale the value in proportion to the Venus crustal thickness). The thermal density difference is given by (Turcotte and Schubert 1982)

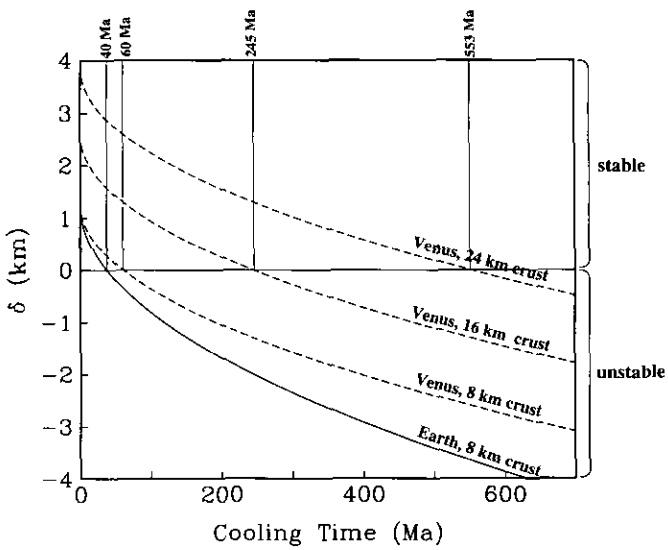

FIG. 11. Density deficit thickness δ (defined in Eq. (2)) as a function of cooling time. A positive value of δ indicates gravitational stability of the lithosphere while a negative value of δ signifies gravitational instability or foundering. The stability of the lithosphere depends on crustal thickness and results are shown for venusian crustal thicknesses of 8, 16, and 24 km (dashed curves). The solid curve is the density deficit thickness vs cooling time for the Earth's oceanic lithosphere with a crustal thickness of 8 km.

$$\delta_{thermal} = -2\alpha(T_m - T_s)\sqrt{\frac{\kappa t}{\pi}}, \tag{3}$$

where α is the thermal expansivity, κ is the thermal diffusivity, T_m is the mantle temperature, T_s is the surface temperature, and t is the cooling time.

Figure 11 presents calculations of δ vs cooling time based on the above for different assumptions about crustal thickness on Venus. The figure also shows δ vs t for the terrestrial lithosphere with a crustal thickness of 8 km. The thermal parameters used in the calculations of Fig. 11 are given in Table III. The value of T_m for Venus is

TABLE III
Parameter Values for Calculation of Lithospheric Buoyancy and Bending Moment

Parameter	Earth	Venus
δ_{comp}	1.3 km	?
T_s	0°C	455°C
T_m	1200°C	1400°C
α	3.1×10^{-5} K^{-1}	3.1×10^{-5} K^{-1}
κ	8.0×10^{-7} m^2 s^{-1}	8.0×10^{-7} m^2 s^{-1}
g	9.8 m s^{-2}	8.9 m s^{-2}
ρ_m	3200 kg m^{-3}	3200 kg m^{-3}
r_0	-	330 km

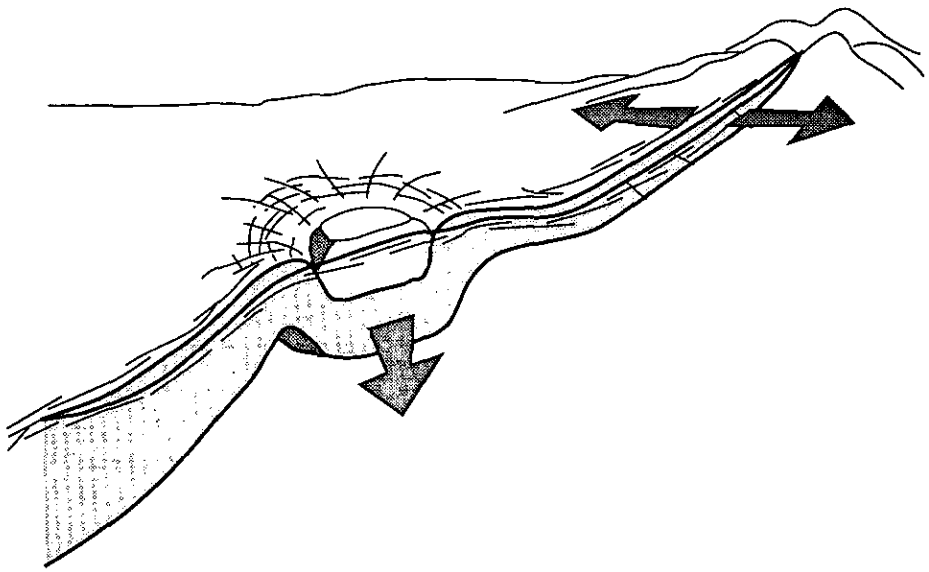

FIG. 12. Sketch illustrating the dual character of a venusian chasma. Near the center of a volcanic rise a chasma has a rift-like appearance and it may be a rift that propagates approximately radially away from the rise center toward lower elevation and into presumably thicker and heavier lithosphere. Far from the rise center, the rift may crack gravitationally unstable lithosphere, permitting foundering or subduction of one or both sides of the lithosphere. At this location the chasma takes on the appearance and character of a subduction zone with an arcuate edge where retrograde subduction is occurring. Oppositely subducting arc segments and replacement of foundered lithosphere with hotter underlying mantle may create structures identified as coronae (e.g., Latona Corona).

based on the assumption that Venus' mantle is dry and has a higher melting point than the Earth's mantle. According to these calculations, the Earth's lithosphere is gravitationally unstable or subductible after 40 Myr. The lithosphere on Venus would be subductible after about 60 Myr for an 8-km-thick crust, after about 245 Myr for a 16-km-thick crust, or after more than 500 Myr for a 24-km-thick crust. These calculations also give minimum times between lithospheric overturn in the episodic model of Turcotte (1993, 1995).

While theoretical calculations allowing for subduction on Venus are encouraging, the case for venusian subduction rests on the observations. The observational evidence in the case of Latona Corona, which shows features attributable to back-arc spreading, is particularly persuasive that subduction is occurring or has occurred on Venus. We have shown that a negatively buoyant subducted slab is needed at southern Latona Corona to balance the large bending moment of the trench and outer rise topography. Subduction at least at one site on Venus (Latona Corona) proves that the venusian lithosphere can be negatively buoyant.

8.3. Duality of Venusian Chasmata

The analysis of the previous section shows that the Venus lithosphere must be old and thick to subduct. Large depths of compensation and geoid–topography ratios at

FIG. 13. (a) Topographic "image" of the Dali–Diana Chasmata system looking northeast toward Atla Regio. Latona Corona is in the foreground. Near Atla Regio the chasmata generally have ridges on both their sides (approximate topographic symmetry similar to terrestrial rifts). Far from Atla Regio, e.g., at Latona Corona, the chasmata generally have high topography on only one of their sides (approximate topographic asymmetry similar to terrestrial subduction zones). The lines are the groundtracks along which topographic profiles shown in (b) were measured. (b) Dashed horizontal lines represent the mean planetary radius of 6051.9 km. The topographic profiles are arranged from top to bottom according to increasing distance from Atla Regio. The topographic profiles illustrate particularly clearly the change in morphology of the chasmata with distance from Atla Regio. The third profile from the top shows the deep trench and high ridge in northern Latona Corona and the two ridges and major outer trench in the southern part of the corona.

FIG. 14. Similar to Fig. 13 but looking northeast along Hecate Chasma toward Beta Regio (a). The topographic profiles shown in (b) are along the groundtracks indicated by the lines in (a) and are arranged from top to bottom according to increasing distance from Beta Regio. Dashed horizontal lines represent the mean planetary radius of 6051.9 km. The southern branch of the chasmata system near Beta Regio is a particularly good example of a rift-like structure with quasi-symmetric ridges on both sides. Farther from Beta Regio, the chasmata change character and have ridges along only one side. A small corona formed by two arcuate segments of the chasma (crossed by the third groundtrack from Beta Regio) is reminiscent of the much larger Latona Corona visible in Fig. 13.

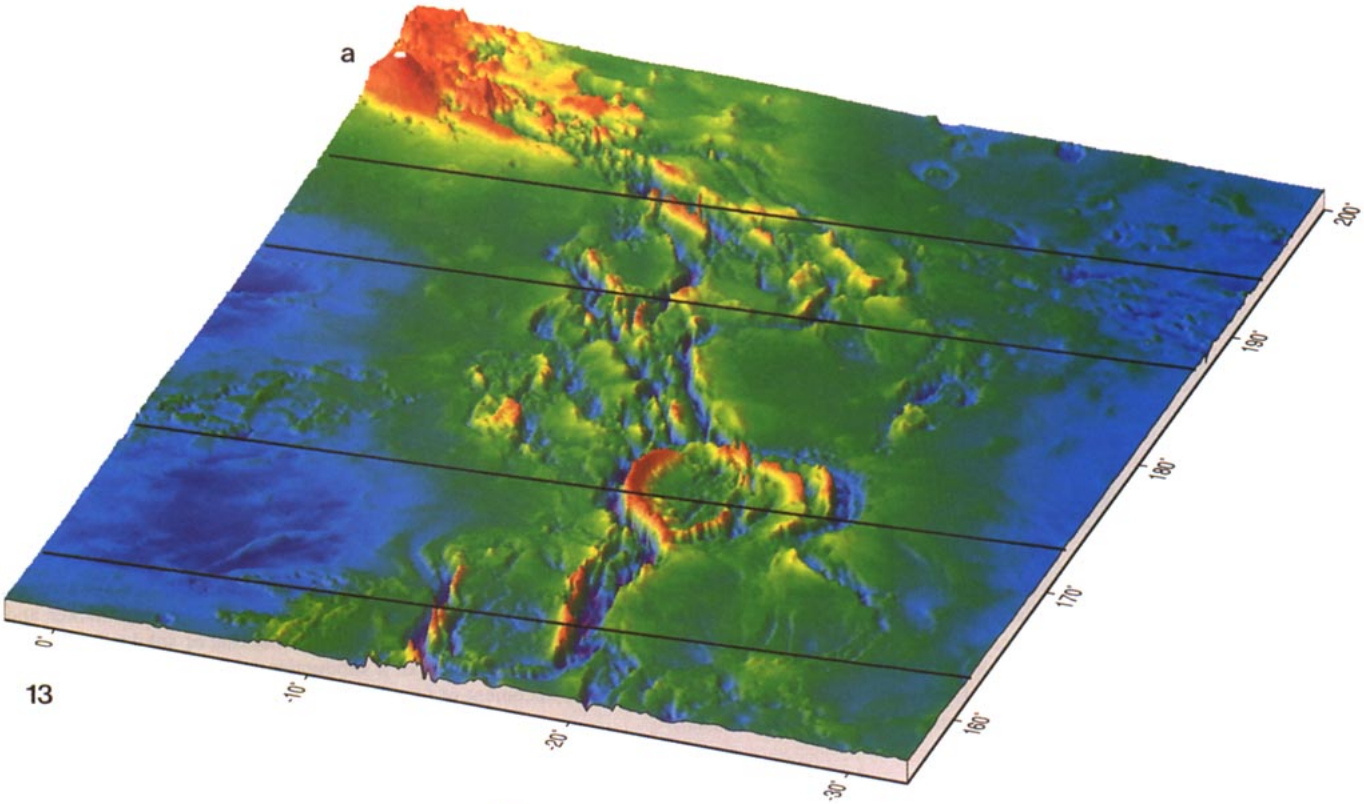

13

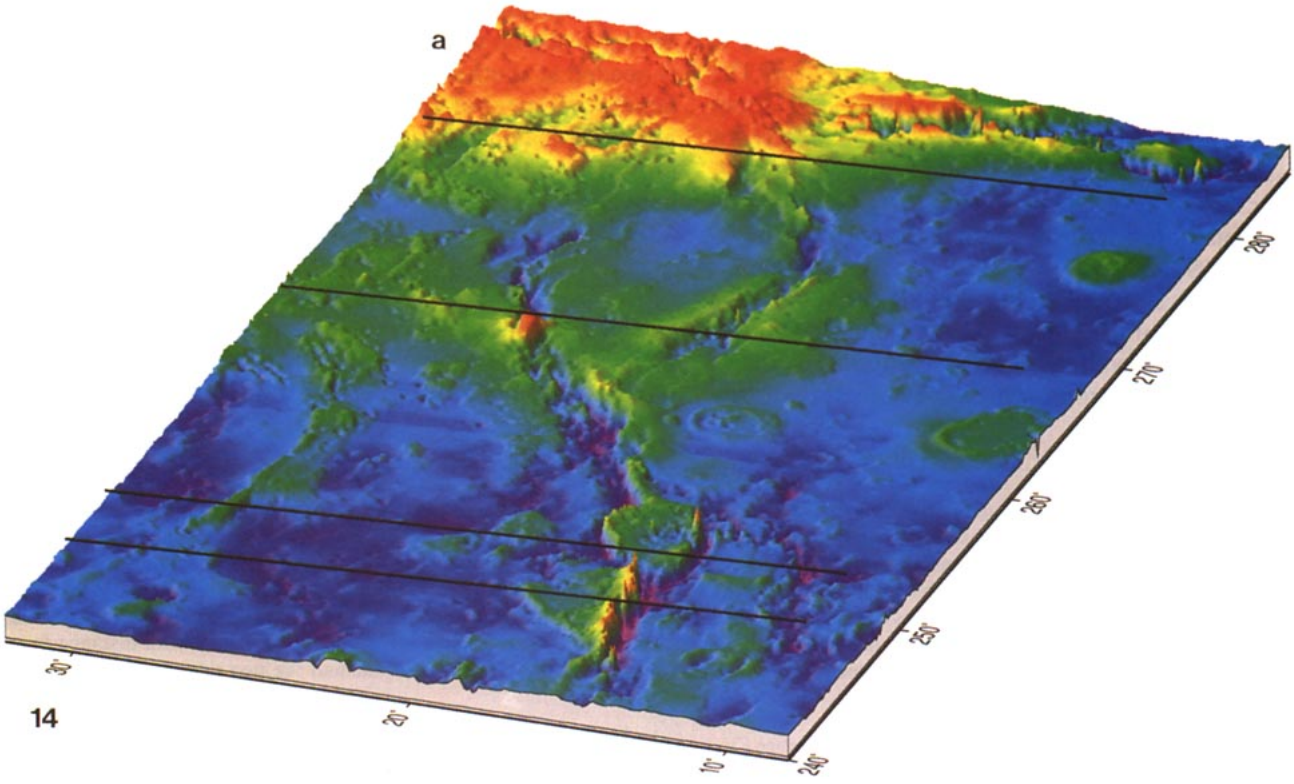

14

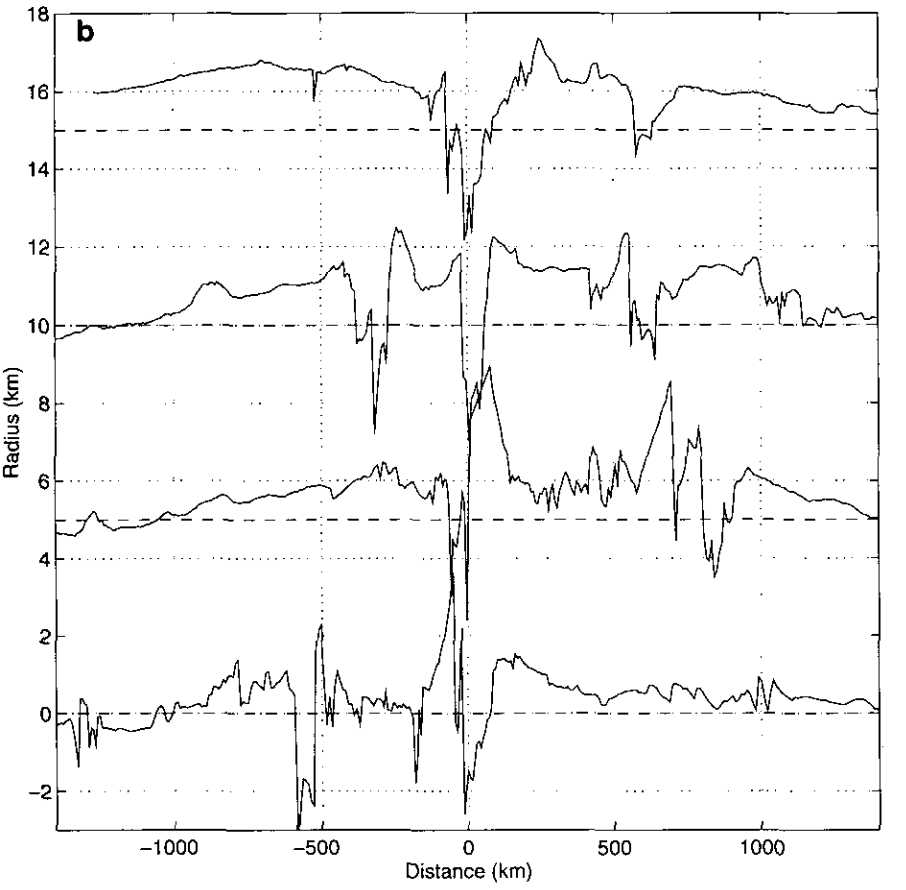
b
Radius (km)
Distance (km)
18
16
14
12
10
8
6
4
2
0
−2
−1000
−500
0
500
1000

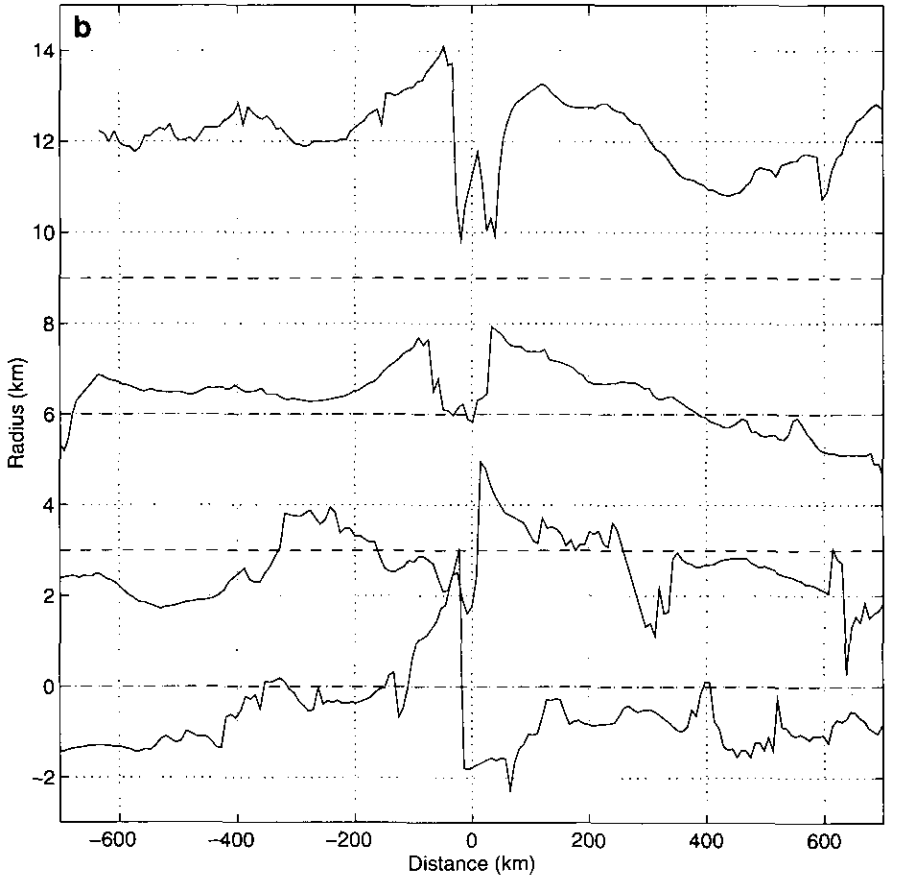
b
Radius (km)
Distance (km)
14
12
10
8
6
4
2
0
−2
−600
−400
−200
0
200
400
600

possible subduction sites (Schubert *et al.* 1994) are consistent with a thick lithosphere at these locations. Large values of elastic thickness inferred from flexural studies of these sites (Table I) are also compatible with a thick lithosphere. Investigations of the global and regional gravity and topography of Venus (e.g., Kuscinkas and Turcotte 1994, Phillips 1994) suggest the possibilty of a planet-wide lithosphere several hundred kilometers thick. How then could subduction be initiated on a planet with such a globally thick lithosphere?

The answer to the question of how subduction could be initiated on Venus may lie in the strong correlation between subduction sites and chasmata and zones of extension. As seen in Fig. 10, many of the subduction sites lie along chasmata systems that extend radially away from the centers of major volcanic rises. The subduction sites at eastern Diana and western Dali Chasmata and at Artemis and Latona Coronae occur along the chasmata system extending southwest from Atla Regio. The subduction site in Parga Chasma occurs along the chasm extending southeast of Atla Regio while the Hecate Chasma subduction site lies along the chasm extending southwest of Beta Regio. Most of the other subduction sites, including Eithinoha, Derceto, and Quetzalpetlatl Coronae, lie along the belt of extension trending north-northeast from Quetzalpetlatl Corona to Derceto Corona. Chasmata are also extensional features, i.e., rifts, near volcanic rises. Three of our proposed subduction sites, Nightingale, Neyterkob, and Demeter, do not occur in association with obvious zones of extension.

Apparently, subduction on Venus occurs in close association with extension or rifting. Before the strong, thick venusian lithosphere can subduct, it must be broken, and only extension and rifting can break the lithosphere. Mature subduction zones on Earth occur far from the major locations of extension and rifting at midocean ridges due to the large horizontal displacements of the plates. On Venus there is no significant horizontal plate motion and subduction and rifting occur in close proximity. Retrograde foundering or subduction of heavy venusian lithosphere occurs in place after rifting or extension has broken or thinned the lithosphere. Rifting or extension of the lithosphere allows the gravitational instability manifest in subduction to take place.

The sketch in Fig. 12 illustrates how subduction might be initiated along a chasma. The chasma is hypothesized to originate as a propagating rift near the center of the uplift of a major volcanic rise. The rift or chasma propagates away from the rise and downhill into lithosphere of increasing thickness. Lithospheric thinning toward the center of a major volcanic rise, perhaps by an underlying mantle plume, is believed to occur on Venus (Moore and Schubert 1995). When the propagating rift encounters lithosphere sufficiently thick to be gravitationally unstable, subduction and rollback of one or both sides of the rift can occur. If there is a cross-rift regional slope, then one-sided subduction would be favored with the edge of the foundering lithosphere migrating downhill. Venusian chasmata may thus have a dual nature as propagating rifts near the centers of volcanic rises and subduction trenches in the lowlands far from the rise centers.

The change in character of venusian chasmata with distance from the center of the volcanic rise is shown in the topographic "images' and profiles of Figs. 13 and 14. The three-dimensional perspectives show the Dali–Diana Chasmata system and Latona Corona looking northeast toward Atla Regio (Fig. 13a) and Hecate Chasma looking northeast toward Beta Regio (Fig. 14a). A series of topographic cross-sections at locations progressively farther from the volcanic rises are shown for the Dali–Diana Chasmata system in Fig. 13b and for Hecate Chasma in Fig. 14b. Near the volcanic rises where the lithosphere is thin and the average elevation is high, the chasmata have the characteristics of rift zones (Solomon *et al.* 1992; Senske *et al.* 1992). Far from the volcanic rises, however, where the average elevation is low, the chasmata have arcuate segments that satisfy the criteria of a possible subduction site.

The small corona along Hecate Chasma (Fig. 14a) bears a striking similarity to the larger Latona Corona (Fig. 13a). Both coronae may have formed by the retrograde rollback of the opposite sides of the chasma, with Latona Corona being larger because of its age or more rapid migration of its outer trench. These coronae are examples of chasma-associated coronae that may be inappropriately identified as circular structures similar to small coronae that are found in the plains away from chasmata. The circular appearance of chasma-associated coronae may be a coincidence of the positions of oppositely subducting arc segments. While small coronae away from chasmata may be fundamentally quasi-circular structures arising from plume-like or diapiric mantle upwellings (Stofan *et al.* 1992, Janes *et al.* 1992) or melt instabilities in broadly upwelling mantle (Tackley and Stevenson 1991, 1993, Tackley *et al.* 1992), the chasma-associated "coronae" may have a totally different origin in subduction. Previously, we proposed that thinning and weakening of the lithosphere by a mantle plume initiated subduction at chasmata-associated coronae such as Artemis Corona and Latona Corona (Sandwell and Schubert 1992a). However, rift initiation of subduction as proposed here makes it unnecessary to explain why these structures are not like the volcanic rises if these coronae were formed by deep mantle plumes. Though there is some volcanism associated with back-arc extension in Latona and Artemis Coronae, there would be much more volcanism and uplift in the interiors if these coronae were above mantle plumes like those at Atla Regio and Beta Regio.

The association of subduction and rifting on the present surface of Venus provides an example of how a massive overturn of the lithosphere might have occurred 500 million years ago (Turcotte 1993, 1995). Had the venusian lithosphere globally thickened to depths of several hundred kilometers it would have effectively thermally blanketed the interior, causing temperatures in the mantle to rise. The higher mantle temperatures may have resulted in hotter and more vigorous plume activity. Plumes incident on the base of the lithosphere would be the only way to break or weaken the lithosphere so that gravitationally unstable lithosphere adjacent to the hotspot sites could sink. Rifting and subduction in close proximity may be a basic result of how Venus loses its heat; rifting and subduction in distant locations is a basic consequence of how Earth loses its heat by plate tectonics.

ACKNOWLEDGMENTS

This work was supported by NASA through grants from the Venus Data Analysis Program (NAGW 3546, NAGW 3503) and the Planetary Geology and Geophysics Program (NAGW 2086). We thank William Moore for his assistance in the preparation of Fig. 12 and Catherine Johnson for modeling many of the flexure profiles.

REFERENCES

BAER, G., G. SCHUBERT, D. L. BINDSCHADLER, AND E. R. STOFAN 1994. Spatial and temporal relations between coronae and extensional belts, northern Lada Terra, Venus. *J. Geophys. Res.* **99,** 8355–8369.

BROWN, C. D., AND R. E. GRIMM 1995. Tectonics of Artemis Chasma: A venusian "plate" boundary. *Icarus*, in press.

BURT, J. D., AND J. W. HEAD 1992. Thermal buoyancy on Venus: Underthrusting vs. subduction. *Geophys. Res. Lett.* **19,** 1707–1710.

CALDWELL, J. G., AND D. L. TURCOTTE 1979. Dependence of the thickness of the elastic oceanic lithosphere on age. *J. Geophys. Res.* **84,** 7572–7576.

FORD, P. G., AND G. H. PETTENGILL 1992. Venus topography and kilometer-scale slopes. *J. Geophys. Res.* **97,** 13,103–13,114.

FUKAO, Y., M. OBAYASHI, H. INOUE, AND M. NENBAU 1992. Subducting slabs stagnant in the mantle transition zone. *J. Geophys. Res.* **97,** 4809–4822.

GARFUNKEL, Z., C. A. ANDERSON, AND G. SCHUBERT 1986. Mantle circulation and the lateral migration of subducted slabs. *J. Geophys. Res.* **91,** 7205–7223.

HANSEN, V. L., AND R. J. PHILLIPS 1993. Tectonics and volcanism of eastern Aphrodite Terra, Venus: No subduction, no spreading. *Science* **260,** 526–530.

ISACKS, B. L., AND M. BARAZANGI 1977. Geometry of Benioff zones: Lateral segmentation and downwards bending of the subducted lithosphere. In *Island Arcs, Deep Sea Trenches, and Back-Arc Basins* (M. Talwani and W. C. Pitman, Eds.,) Maurice Ewing Series 1, pp. 99–114. Am. Geophys. Union, Washington, DC.

JANES, D. M., S. W. SQUYRES, D. L. BINDSCHADLER, G. BAER, G. SCHUBERT, V. L. SHARPTON, AND E. R. STOFAN 1992. Geophysical models for the formation and evolution of coronae on Venus. *J. Geophys. Res.* **97,** 16,055–16,067.

JOHNSON, C. L., AND D. T. SANDWELL 1994. Lithospheric flexure on Venus, *Geophys. J. Int.* **119,** 627–647.

KIRBY, S. H. 1983. Rheology of the lithosphere. *Rev. Geophys.* **21,** 1458–1487.

KUSCINKAS, A. B., AND D. L. TURCOTTE 1994. Isostatic compensation of equatorial highlands on Venus. *Icarus* **112,** 104–116.

LEVITT, D. A., AND D. T. SANDWELL 1995. Lithospheric bending at subduction zones based on depth soundings and satellite gravity. *J. Geophys. Res.* **100,** 379–400.

MACKWELL, S. J., M. E. ZIMMERMAN, D. L. KOHLSTEDT, AND D. S. SCHERBER 1995. Experimental deformation of dry columbia diabase: Implications for tectonics on Venus. In *Proceedings, 35th U.S. Symposium on Rock Mechanics, Lake Tahoe, NV.* (J. J. K. Daemen and R. A. Schultz, Eds.), pp. 207–214.

MASSON, D. G. 1991. Fault patterns at outer trench walls. *Mar. Geophys. Res.* **13,** 209–225.

MAURICE, K. E., AND J. C. CURLANDER 1994. *Magellan Stereo Toolkit User Manual Rel. Version 1.2.2,* Vexcel Co.

MCADOO, D. C. 1981. Geoid anomalies in the vicinity of subduction zones, *J. Geophys. Res.* **86,** 6073–6090.

MCADOO, D. C., J. G. CALDWELL, AND D. L. TURCOTTE 1978. On the elastic-perfectly plastic bending of the lithosphere under generalized loading with application to the Kurile trench. *Geophys. J. R. Astron. Soc.* **54,** 11–26.

MCKENZIE, D., P. G. FORD, C. JOHNSON, B. PARSONS, D. SANDWELL, S. SAUNDERS, AND S. C. SOLOMON 1992. Features on Venus generated by plate boundary processes. *J. Geophys. Res.* **97,** 13,533–13,544.

MCNUTT, M. K. 1984. Lithospheric flexure and thermal anomalies. *J. Geophys. Res.* **89,** 11,180–11,194.

MCNUTT, M. K., AND H. W. MENARD 1982. Constraints on yield strength in the oceanic lithosphere derived from observations of flexure. *Geophys. J. R. Astron. Soc.* **71,** 363–394.

MCQUEEN, H. W. S., AND K. LAMBECK 1989. The accuracy of some lithospheric bending parameters. *Geophys. J.* **96,** 401–413.

MOORE, W. B., AND G. SCHUBERT 1995. Lithospheric thickness and mantle/lithosphere density contrast beneath Beta Regio, Venus. *Geophys. Res. Lett.* **22,** 429–432.

MUELLER, S., AND R. J. PHILLIPS 1995. On the reliability of lithospheric constraints derived from elastic models of outer-rise flexure. *Geophys. J. Int.*, in press.

MUELLER, S., AND R. J. PHILLIPS 1991. On the initiation of subduction. *J. Geophys. Res.* **96,** 651–665.

OXBURGH, E. R., AND E. M. PARMENTIER 1977. Compositional and density stratification in the oceanic lithosphere—causes and consequences. *J. Geol. Soc. London* **133,** 343–354.

PARSONS, B., AND P. MOLNAR 1976. The origin of outer topographic rises associated with trenches. *Geophys. J. R. Astron. Soc.* **45,** 707–712.

PHILLIPS, R. J. 1994. Estimating lithospheric properties at Atla Regio, Venus. *Icarus* **112,** 147–170.

PHILLIPS, R. J., AND M. C. MALIN 1983. The interior of Venus and tectonic implications. In *Venus* (D. M. Hunten, L. Colin, T. M. Donahue, and V. I. Moroz, Eds.) pp. 159–214, Univ. of Arizona Press, Tucson.

REYMER, A., AND G. SCHUBERT 1984. Phanerozoic addition rates to the continental crust and crustal growth. *Tectonics* **3,** 63–77.

ROEDER, D. H. 1975. Tectonic effects of dip changes in subduction zones. *Am. J. Sci.* **275,** 252–264.

SANDWELL, D. T., AND G. SCHUBERT 1992a. Evidence for retrograde lithospheric subduction on Venus. *Science* **257,** 766–770.

SANDWELL, D. T., AND G. SCHUBERT 1992b. Flexural ridges, trenches,

and outer rises around coronae on Venus. *J. Geophys. Res.* **97,** 16,069–16,083.

SCHABER, G. G., R. G. STROM, H. J. MOORE, L. A. SODERBLOM, R. L. KIRK, D. J. CHADWICK, D. D. DAWSON, L. R. GADDIS, J. M. BOYCE, AND J. RUSSELL 1992. Geology and distribution of impact craters on Venus: What are they telling us? *J. Geophys. Res.* **97,** 13,257–13,301.

SCHUBERT, G., W. B. MOORE, AND D. T. SANDWELL 1994. Gravity over coronae and chasmata on Venus. *Icarus* **112,** 130–146.

SENSKE, D. A., G. G. SCHABER, AND E. R. STOFAN 1992. Regional topographic rises on Venus: Geology of western Eistla Regio and comparison to Beta Regio and Atla Regio. *J. Geophys. Res.* **47,** 13,395–13,420.

SOLOMON, S. C., AND J. W. HEAD 1990. Lithospheric flexure beneath the Freyja Montes foredeep, Venus: Constraints on lithospheric thermal gradient and heat flow. *Geophys. Res. Lett.* **17,** 1393–1396.

SOLOMON, S. C., J. W. HEAD, W. M. KAULA, D. MCKENZIE, B. PARSONS, R. J. PHILLIPS, G. SCHUBERT, AND M. TALWANI 1991. Venus tectonics: Initial analysis from Magellan. *Science* **252,** 297–312.

SOLOMON, S. C., P. J., MCGOVERN, M. SIMONS, AND J. W. HEAD 1994. Gravity anomalies over volcanoes on Venus: Implications for lithospheric thickness and volcano history. *Proc. Lunar Planet. Sci. Conf. 8th,* 1317–1318.

SOLOMON, S. C., S. E. SMREKAR, D. L. BINDSCHADLER, R. E. GRIMM, W. M. KAULA, G. E. MCGILL, R. J. PHILLIPS, R. S. SAUNDERS, G. SCHUBERT, S. W. SQUYRES, AND E. R. STOFAN 1992. Venus tectonics: An overview of Magellan observations. *J. Geophys. Res.* **97,** 13,199–13,255.

SQUYRES, S. W., D. M. JANES, G. BAER, D. L. BINDSCHADLER, G. SCHUBERT, V. L. SHARPTON, AND E. R. STOFAN 1992. The morphology and evolution of coronae on Venus. *J. Geophys. Res.* **97,** 13,611–13,634.

STOFAN, E. R., AND J. W. HEAD 1990. Coronae of Mnemosyne Regio, Venus: Morphology and origin. *Icarus* **83,** 216–243.

STOFAN, E. R., V. L. SHARPTON, G. SCHUBERT, G. BAER, D. L. BINDSCHADLER, D. M. JANES, AND S. W. SQUYRES 1992. Global distribution and characteristics of coronae and related features on Venus: Implications for origin and relation to mantle processes. *J. Geophys. Res.* **97,** 13,347–13,378.

SUPPE, J., AND C. CONNERS 1992. Critical taper wedge mechanics of fold-and-thrust belts on Venus: Initial results from Magellan. *J. Geophys. Res.* **97,** 13,545–13,561.

TACKLEY, P. J., AND D. J. STEVENSON 1993. A mechanism for spontaneous self-perpetuating volcanism on the terrestrial planets. In *Flow and Creep in the Solar System: Observations, Modelling and Theory* (E. B. Stone and S. K. Runcorn, Eds.), pp. 307–321. Kluwer, Dordrecht, Netherlands.

TACKLEY, P. J., AND D. J. STEVENSON 1991. The production of small Venusian coronae by Rayleigh–Taylor instabilities in the uppermost mantle. *EOS Trans. AGU Supplement,* Vol. 72, No. 44, p. 287. Abstract.

TACKLEY, P. J., D. J. STEVENSON, AND D. R. SCOTT 1992. Volcanism by melt-driven Rayleigh–Taylor instability and possible consequences of melting for admittance ratios on Venus. In *Papers Presented to the International Colloquium on Venus, Lunar and Planetary Institute Contribution* No. 789, pp. 123–124.

TURCOTTE, D. L. 1995. How does Venus lose its heat? *J. Geophys. Res.,* in press.

TURCOTTE, D. L. 1993. An episodic hypothesis for Venusian tectonics. *J. Geophys. Res.* **98,** 17,061–17,068.

TURCOTTE, D. L., AND G. SCHUBERT 1982. *Geodynamics.* Wiley, New York.

VAN DER HILST, R., R. ENGDAHL, W. SPAKMAN, AND G. NOLET 1991. Tomographic imaging of subducted lithosphere below northwest Pacific island arcs. *Nature* **353,** 37–43.

WESSEL, P. 1992. Thermal stress and the biomodal distribution of elastic thickness estimates of the oceanic lithosphere. *J. Geophys. Res.* **97,** 14,177–14,193.